Analysis of the Dynamics in Linear Chain Models by means of Generalized Langevin Equations

Fabian Koch[1] · Suvendu Mandal[2] · Tanja Schilling[1]

Abstract

We analyse the motion of one particle in a polymer chain. For this purpose, we use the framework of the exact (non-stationary) generalized Langevin equation that can be derived from first principles via the projection-operator method. Our focus lies on determining memory kernels from either exact expressions for autocorrelation functions or from simulation data. We increase the complexity of the underlying system starting out from one-dimensional harmonic chains and ending with a polymer driven through a polymer melt. Here, the displacement or the velocity of an individual particle in the chain serves as the observable. The central result is that the time-window in which the memory kernels show structure before they rapidly decay decreases with increasing complexity of the system.

1 Introduction

The dynamics of microscopic systems is time-local – be they described classically by Hamilton's equations of motion or quantum-mechanically by the Schrödinger equation. If one integrates out some degrees of freedom to obtain effective equations of motion for the remaining degrees of freedom, the resulting equations are in general non-local in time [1–3]. However, experience shows that often time-local effective equations of motion such as the Markovian Langevin equation produce very good approximations to the true dynamics. One might therefore wonder where and how the memory effects vanish.

Polymer melts seem to be perfect model systems to study memory, because their dynamics are governed by a large range of different time-scales and their rheological behaviour is clearly dominated by memory effects. When integrating out the motion of most monomer units in

---

Communicated by Ludovic Berthier.

✉ Fabian Koch
  fabian.glatzel@physik.uni-freiburg.de

  Suvendu Mandal
  suvendu.mandal@pkm.tu-darmstadt.de

  Tanja Schilling
  tanja.schilling@physik.uni-freiburg.de

[1] Institute of Physics, University of Freiburg, Hermann-Herder-Str. 3, 79104 Freiburg, Germany

[2] Institut für Physik kondensierter Materie, Technische Universität Darmstadt, Hochschulstraße 8, D-64289 Darmstadt, Germany

a polymer chain in order to obtain an equation of motion for one (or a few) monomer units, one expects to see traces of the different relaxation time-scales, the Rouse times [4], in the memory kernel. In this article we show that the structure of the memory kernel at short times is dominated by other factors such as the collision patterns among the monomers. Numerical evidence displayed in this article shows that the time window of this short-time structure decreases with the complexity of the system. Further, the long-time tails of the memory kernels responsible for phenomena like the subdiffusive regime in the mean square displacement are strongly suppressed and easily lost in statistical or numerical noise.

In order to rationalize this finding we discuss the equations of motion of the harmonic chain with and without constrained ends. We systematically increase the complexity of the problem by going from one dimension to higher dimensions, adding anharmonic contributions and considering driven systems. In all cases we construct the generalized Langevin equation for the position and velocity of one particle in the chain and compute the corresponding memory kernel.

Similar approaches have already yielded valuable insights regarding the long-time tails of velocity auto-correlation functions [5], the delocalization-localization transition [6], non-Clausius heat transfer [7] and coarse graining of harmonic lattices [8]. For example, in ref. [9] the collision of a single particle with a harmonic chain is studied. This work illustrates that analytic results for the generalized Langevin equation can be obtained if one starts out from the purely harmonic case. Other works investigate memory functions for chain models that include stochasticity already at the microscopy level [10]. One famous special example for this is the Rouse model. In ref. [11] collective properties such as Onsager coefficents are derived for the Rouse model and in ref. [12] effective equations of motions for monomers are derived via an induction scheme along the model polymer chains.

In our work, we start out from the deterministic harmonic case and then analyse changes in the memory kernels with increasing complexity of the model. The only time we explicitly use a stochastic model, namely the Rouse model with inertia, is in the context of interpreting our findings for the deterministic polyme-melt system. We show that long-time memory is easily lost when different kinds of anharmonicity are introduced. Further, we show that adding intermolecular interactions to the intramolecular ones does not alter the shape of the memory kernels qualitatively.

Many materials properties of polymer melts are not accessible by fully atomistic computer simulations, because of high computational costs. Hence, there has been considerable effort in constructing effective descriptions for multi-scale modelling of polymers [13–18]. In this context it is relevant to understand when coarse-graining introduces memory, thus our study might also serve as a basis in this field.

The structure of the article is as follows: In Section 2 we recapitulate the fundamental results of the projection operator technique in the context of the generalized Langevin equation. In Section 3 and Section 4 we derive the analytic solutions for the dynamics in a (free) harmonic chain and in Section 5 we do so for the Rouse model with inertia. In Section 6 we show and discuss the different quantities appearing in the generalized Langevin equation for our different (model) systems (see fig. 1). In Section 6.1 we discuss the purely harmonic chain in one dimension with both fixed and free ends, in Section 6.2 an anharmonic Weeks-Chandler-Anderson interaction potential is added. Next, in Section 6.3 we analyze the free chains with and without anharmonicity in two and three dimensions. Finally we regard a polymer melt in and out of equilibrium and compare it with the Rouse model with inertia in Section 6.4. We summarize our findings in Section 7.

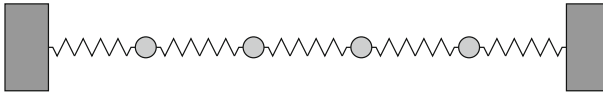**Sec. 6.1**:
1D, harmonic, fixed or free ends
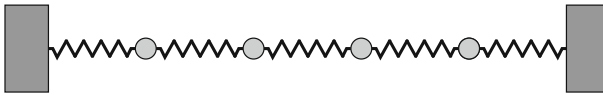
− or −

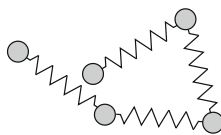**Sec. 6.2**:
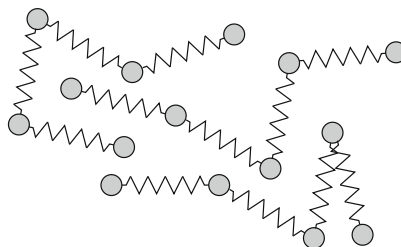1D, anharmonic, fixed or free ends

− or −

Sec. 6.3:
2D/3D, anharmonic, free ends

Sec. 6.4:
3D, anharmonic, melt

Fig. 1 Sketches of the model systems discussed in Section 6. The complexity is increased stepwise. Starting from an one-dimensional harmonic-oscillator chain in Section 6.1, anharmonicities are added in Section 6.2, then systems in two or three dimensions are considered in Section 6.3, and finally a complete polymer melt is regarded in Section 6.4

2 Generalized Langevin Equation

Given a system with Hamiltonian dynamics, a Liouvillian $\mathcal{L}$, and an observable that is a function of phase space $A(\Gamma)$, one can derive an equation of motion for A via the projection operator formalism [19, 20]. In case the Liouvillan or the observable explicitly depend on time, one can use a generalized, time-dependent Mori projector [21, 22] to obtain the non-stationary generalized Langevin equation (nsGLE)

$$\frac{dA(t)}{dt} = \omega(t)A(t) - \int_0^t d\tau \, K(t, \tau)A(\tau) + \eta(0, t). \tag{1}$$

with

$$\omega(t) := (\mathcal{L}A, A)_t \, (A, A)_t^{-1}, \tag{2}$$

$$K(t, \tau) := -\left((\mathcal{L} - \dot{\mathcal{P}}(\tau))\mathcal{Q}(\tau)\mathcal{G}(\tau, t)\mathcal{L}A, A\right)_\tau (A, A)_\tau^{-1}, \tag{3}$$

$$\eta(t', t) := \exp\left(\mathcal{L}t'\right) \mathcal{Q}(t')\mathcal{G}(t', t)\mathcal{L}A(\Gamma). \tag{4}$$

Here, $\mathcal{P}(t)$ is the time-dependent projection operator defined through

$$\mathcal{P}(t)X(\Gamma) := \frac{(X, A)_t}{(A, A)_t} A(\Gamma), \tag{5}$$

$\mathcal{Q}(t) = 1 - \mathcal{P}(t)$ is its orthogonal complement and $\mathcal{G}(t', t)$ is defined through

$$\mathcal{G}(t', t) := \exp_-\left(\int_{t'}^t d\tau \, \mathcal{L}\mathcal{Q}(\tau)\right), \tag{6}$$

where $\exp_-(\cdots)$ denotes the negatively time-ordered exponential. The parentheses with the subscript denote the scalar product of phase-space functions

$$(X, Y)_t := \int d\Gamma \rho(\Gamma, t)X(\Gamma)Y(\Gamma). \tag{7}$$

Further, one can show that the memory kernel $K(t, \tau)$ and the (deterministic) fluctuating forces $\eta(t', t)$ fulfill a relation similar to a fluctuation-kernel theorem, namely

$$K(t, \tau) = \left(\eta(t', t), \eta(t', \tau)\right)_{t'} (A, A)_\tau^{-1}. \tag{8}$$

The memory kernel can be computed from the correlation function $C(t, t') = \langle A(t)A(t')\rangle$ using the relation

$$\frac{\partial}{\partial t}C(t, t') = \omega(t)C(t, t') - \int_0^t d\tau \, K(t, \tau)C(\tau, t'). \tag{9}$$

Note that the fluctuating force does not appear in this equation, because $\langle \eta(0, t)A(0)\rangle = 0 \; \forall \, t$. An efficient algorithm to extract the drift and the memory kernel from the correlation function is introduced in ref. [23].

All these results are exact, i.e. they do not require assumptions on time-scale separation or "relevant" observables. They can be derived for driven systems with explicitly time-dependent Hamiltonians/Liouvillians and/or observables [22], for dynamics subject to holonomic constraints, and for vectorial observables [24].

If the phase-space distribution is stationary, both the correlation function and the memory kernel can be expressed as a function of a single variable. Further, the drift term $\omega(t)$ vanishes if no vectorial observables are considered. In this case the stationary generalized Langevin equation reads [1, 25–28]

$$\frac{dA(t)}{dt} = -\int_0^t d\tau \, K(t - \tau)A(\tau) + \eta(t). \tag{10}$$

Again, by using the orthogonality of the fluctuating force $\eta(t)$ and the observable $A(0)$, we can derive the following equation for the covariance

$$\frac{dC(t)}{dt} = -\int_0^t d\tau \, K(t-\tau)C(\tau), \tag{11}$$

where the correlation function does only depend on the time difference of the two "measurements" $C(t) := C(t', t' + t)$. Via a Laplace transform we obtain (cf. the original article by Mori [1])

$$\tilde{K}(s) = \frac{C(0) - s\tilde{C}(s)}{\tilde{C}(s)}. \tag{12}$$

Hence, for a scalar-valued observable and a system under stationary conditions, the auto-correlation function of the observable contains all information needed to reconstruct the exact generalized Langevin equation: the memory kernel follows from eq. (11) and the drift is zero.

By calculating the time derivative of eq. (11) one can derive an expression that allows to gain some insight in the structure of the memory kernel

$$K(t) = -\frac{\ddot{C}(t)}{C(0)} - \frac{1}{C(0)} \int_0^t d\tau \, K(\tau)\dot{C}(t-\tau). \tag{13}$$

As the last term is expected to be small for small t, the first term on the right-hand side, which can easily be interpreted, may yield a good approximation of the memory kernel on short time scales.

In the following we add a subscript "vel" or "dis" to the correlation functions and memory kernels to specify the observable as velocity or displacement. Further, we add a superscript "b" or "f" for bound (implying fixed ends) or free chains.

3 Harmonic Chain

As an introduction to the topic, we first recall the derivations from ref. [29] and add some minor corrections. Section IV of ref. [29] deals with the displacement and velocity autocorrelation function of a one-dimensional harmonic-oscillator chain with fixed-end boundary conditions. Let q_n denote the displacement (with respect to the equilibrium position) and p_n the momentum of the n-th particle. The Hamiltonian of such a chain with N particles (see the sketch labeled "Sec. 6.1" in fig. 1) reads

$$H = \frac{1}{2m} \sum_{n=1}^{N} p_n(t)^2 + \frac{k}{2} \sum_{n=0}^{N} (q_n(t) - q_{n+1}(t))^2. \tag{14}$$

Thus, the equations of motion for the n-th particle are

$$\dot{q}_n(t) = \frac{p_n(t)}{m}, \tag{15}$$

$$\dot{p}_n(t) = k(q_{n-1}(t) - 2q_n(t) + q_{n+1}(t)). \tag{16}$$

Here we set $q_0(t) = q_{N+1}(t) = 0$ (fixed ends). (Note that the interaction term, i.e. the second term in the Hamiltonian, contains a sum over all pairs of particles. This is not a model of the Kac–Zwanzig type [30].

Via a discrete sine transform, one can now switch to a set of new generalized coordinates and momenta that diagonalize the Hamiltonian [29] (note that in the referenced article prefactors of $\sqrt{2}$ are missing in the transformation and thus the final result is only correct up to a factor of two)

$$\tilde{q}_j(t) := \sqrt{\frac{2m}{N+1}} \sum_{n=1}^{N} q_n(t) \sin\left(\frac{\pi nj}{N+1}\right), \tag{17}$$

$$\tilde{p}_j(t) := \sqrt{\frac{2}{(N+1)m}} \sum_{n=1}^{N} p_n(t) \sin\left(\frac{\pi nj}{N+1}\right) \tag{18}$$

and the inverse transform

$$q_j(t) = \sqrt{\frac{2}{(N+1)m}} \sum_{n=1}^{N} \tilde{q}_n(t) \sin\left(\frac{\pi nj}{N+1}\right), \tag{19}$$

$$p_j(t) = \sqrt{\frac{2m}{N+1}} \sum_{n=1}^{N} \tilde{p}_n(t) \sin\left(\frac{\pi nj}{N+1}\right). \tag{20}$$

Thus, all discrete sine transforms here are of the type "DST-I" [31, 32]. The Hamiltonian for the new coordinates reads

$$H = \frac{1}{2} \sum_{n=1}^{N} \tilde{p}_n^2 + \frac{1}{2} \sum_{n=1}^{N} \Omega_n^2 \tilde{q}_n^2 \tag{21}$$

with the normal-mode frequencies

$$\Omega_n = 2\sqrt{\frac{k}{m}} \sin\left(\frac{\pi n}{2(N+1)}\right). \tag{22}$$

The point transformation above preserves the canonical structure of the equations of motion and hence

$$\dot{\tilde{q}}_j = \frac{\partial H}{\partial \tilde{p}_j} = \tilde{p}_j, \tag{23}$$

$$\dot{\tilde{p}}_j = -\frac{\partial H}{\partial \tilde{q}_j} = -\Omega_j^2 \tilde{q}_j. \tag{24}$$

Solving these partial differential equations yields

$$\tilde{q}_j(t) = \tilde{q}_j(0)\cos(\Omega_j t) + \frac{\tilde{p}_j(0)}{\Omega_j}\sin(\Omega_j t), \tag{25}$$

$$\tilde{p}_j(t) = \tilde{p}_j(0)\cos(\Omega_j t) - \Omega_j \tilde{q}_j(0)\sin(\Omega_j t). \tag{26}$$

Turning towards autocorrelation functions one can write

$$\langle q_j(t)q_j(0)\rangle = \frac{2}{(N+1)m} \sum_{n,n'=1}^{N} \langle \tilde{q}_n(t)\tilde{q}_{n'}(0)\rangle \sin\left(\frac{\pi nj}{N+1}\right)\sin\left(\frac{\pi n'j}{N+1}\right), \tag{27}$$

$$\langle p_j(t)p_j(0)\rangle = \frac{2m}{(N+1)} \sum_{n,n'=1}^{N} \langle \tilde{p}_n(t)\tilde{p}_{n'}(0)\rangle$$

$$\times \sin\left(\frac{\pi n j}{N+1}\right)\sin\left(\frac{\pi n' j}{N+1}\right). \tag{28}$$

Now, we can determine the correlation functions in a canonical ensemble

$$\langle \tilde{q}_n(t)\tilde{q}_{n'}(0)\rangle = \frac{1}{Z}\int d\Gamma \exp(-\beta H)$$

$$\times \left(\tilde{q}_n(0)\cos(\Omega_n t) + \frac{\tilde{p}_n(0)}{\Omega_n}\sin(\Omega_n t)\right)\tilde{q}_{n'}(0) \tag{29}$$

$$= \frac{\delta_{nn'}\cos(\Omega_n t)}{Z}\int d\Gamma \exp(-\beta H)\tilde{q}_n(0)^2 \tag{30}$$

$$= \delta_{nn'}\cos(\Omega_n t)\frac{1}{\beta\Omega_n^2} \tag{31}$$

and analogously

$$\langle \tilde{p}_n(t)\tilde{p}_{n'}(0)\rangle = \delta_{nn'}\cos(\Omega_n t)\frac{1}{\beta}. \tag{32}$$

Inserting these expressions into the equations above yields

$$\langle q_j(t)q_j(0)\rangle = \frac{2k_B T}{(N+1)m}\sum_{n=1}^{N}\sin^2\left(\frac{\pi n j}{N+1}\right)\frac{\cos(\Omega_n t)}{\Omega_n^2}, \tag{33}$$

$$\langle p_j(t)p_j(0)\rangle = \frac{2mk_B T}{N+1}\sum_{n=1}^{N}\sin^2\left(\frac{\pi n j}{N+1}\right)\cos(\Omega_n t), \tag{34}$$

or if we are interested in the covariance of the velocity

$$\langle v_j(t)v_j(0)\rangle = \frac{\langle p_j(t)p_j(0)\rangle}{m^2} \tag{35}$$

$$= \frac{2k_B T}{(N+1)m}\sum_{n=1}^{N}\sin^2\left(\frac{\pi n j}{N+1}\right)\cos(\Omega_n t). \tag{36}$$

The same result can be derived by using the connection between the displacement and velocity correlation function in a stationary ensemble

$$\langle v_j(t)v_j(0)\rangle = -\frac{d^2\langle q_j(t)q_j(0)\rangle}{dt^2}. \tag{37}$$

In the thermodynamic limit of $N \to \infty$ the sums can be replaced by integrals. Solving these integrals, ref. [29] finds

$$\langle v_j(t)v_j(0)\rangle = \frac{k_B T}{m}[J_0(2\omega t) - J_{4j}(2\omega t)] \tag{38}$$

where J_n is the n-th Bessel function and $\omega = \sqrt{k/m}$.

4 Free Harmonic Chain

Considering a harmonic chain with no fixed ends, one can follow a similar derivation as for the one with fixed ends. First, the Hamiltonian for a free chain with N particles reads

$$H = \frac{1}{2m} \sum_{n=1}^{N} p_n(t)^2 + \frac{k}{2} \sum_{n=1}^{N-1} (q_n(t) - q_{n+1}(t))^2. \tag{39}$$

To diagonalize the Hamiltonian we use the discrete cosine transformation "DCT-II" [31, 32]

$$\tilde{q}_j(t) := \sqrt{\frac{2}{N}} \sum_{n=1}^{N} q_n(t) \cos\left(\frac{\pi (n - \frac{1}{2})j}{N}\right), \tag{40}$$

$$\tilde{p}_j(t) := \sqrt{\frac{2}{N}} \sum_{n=1}^{N} p_n(t) \cos\left(\frac{\pi (n - \frac{1}{2})j}{N}\right), \tag{41}$$

and the inverse transfomations, the "DCT-III" [31, 32],

$$q_j(t) = \sqrt{\frac{2}{N}} \left(\frac{1}{2}\tilde{q}_0(t) + \sum_{n=1}^{N-1} \tilde{q}_n(t) \cos\left(\frac{\pi n \left(j - \frac{1}{2}\right)}{N}\right)\right), \tag{42}$$

$$p_j(t) = \sqrt{\frac{2}{N}} \left(\frac{1}{2}\tilde{p}_0(t) + \sum_{n=1}^{N-1} \tilde{p}_n(t) \cos\left(\frac{\pi n \left(j - \frac{1}{2}\right)}{N}\right)\right). \tag{43}$$

Note that the equations for the transformations differ slightly from the usual "DCT-II" and "DCT-III" because the first particle in the chain has the index 1 instead of 0. The Hamiltonian in the new coordinates reads

$$H = \frac{\tilde{p}_0^2}{4m} + \sum_{n=1}^{N-1} \frac{\tilde{p}_n^2}{2m} + \sum_{n=1}^{N-1} \frac{m\Omega_n^2 \tilde{q}_n^2}{2} \tag{44}$$

with

$$\Omega_n := 2\sqrt{\frac{k}{m}} \sin\left(\frac{\pi n}{2N}\right). \tag{45}$$

The corresponding equations of motion are

$$\dot{\tilde{q}}_0 = \frac{\tilde{p}_0}{m}, \qquad \dot{\tilde{p}}_0 = 0, \tag{46}$$

$$\dot{\tilde{q}}_n = \frac{\tilde{p}_n}{m}, \qquad \dot{\tilde{p}}_n = -m\Omega_n^2 \tilde{q}_n \quad \text{for } 1 \leq n < N \tag{47}$$

and are solved by

$$\tilde{q}_0(t) = \tilde{q}_0(0) + \frac{\tilde{p}_0(0)}{m}t, \tag{48}$$

$$\tilde{p}_0(t) = \tilde{p}_0(0), \tag{49}$$

and for $1 \leq n < N$

$$\tilde{q}_n(t) = \tilde{q}_n(0) \cos(\Omega_n t) + \frac{\tilde{p}_n(0)}{m\Omega_n} \sin(\Omega_n t), \tag{50}$$

$$\tilde{p}_n(t) = -m\Omega_n \tilde{q}_n(0)\sin(\Omega t) + \tilde{p}_n(0)\cos(\Omega t). \tag{51}$$

The correlation functions can be calculated in the same fashion as for the chain with fixed ends and we obtain for example

$$\langle \tilde{p}_n(t)\tilde{p}_{n'}(0)\rangle = \delta_{nn'}(1 + \delta_{n0})\frac{m}{\beta}. \tag{52}$$

5 Rouse Model with Inertia

Another model that can be tackled partly by an analytical approach is the well established Rouse model for polymers [33]. This model has been used with a variety of versions of the generalized Langevin equation to describe for example the dynamics of the end-to-end distance [34], the dynamics of the central particle in the chain [35], or the response of an end monomer to external forcing [36]. Note that the structure of the generalized Langevin equation in the last reference stems from an iterative ansatz and differs from our one in important aspects, e.g. it does not satisfy the fluctuation-kernel theorem by construction.

In contrast to the original form of the Rouse model, we choose a version that includes inertia in order to obtain a momentum-autocorrelation function. The equations of motion for the different spatial dimensions decouple and are, thus, independent. Hence, we use the notation for a one-dimensional system to avoid cluttering the equations with additional indices. The equations of motion for a Rouse chain of length N with inertia read

$$\dot{q}_n(t) = \frac{p_n(t)}{m}, \tag{53}$$

$$\dot{p}_n(t) = k(q_{n-1}(t) - 2q_n(t) + q_{n+1}(t)) - \gamma p_n(t) + \xi_n(t) \tag{54}$$

for the particles that are not at the ends of the chain. For the end particles the second equation of motion is replaced by

$$\dot{p}_1(t) = k(-q_1(t) + q_2(t)) - \gamma p_1(t) + \xi_1(t), \tag{55}$$

$$\dot{p}_N(t) = k(q_{N-1}(t) - q_N(t)) - \gamma p_N(t) + \xi_N(t). \tag{56}$$

Here, γ is an effective friction constant and $\xi_n(t)$ is a Gaussian white noise with zero mean and an autocorrelation of

$$\langle \xi_n(t)\xi_m(t')\rangle = 2\gamma m k_B T \delta(t - t')\delta_{nm}. \tag{57}$$

The effective friction and the noise model the solvent implicitly. Thus, the results derived in this subsection are used in section 6.4 in the context of polymer melts where the other polymers may be regarded as an origin of "noise".

We briefly derive the analytic expression for the momentum-autocorrelation functions here. A derivation for the Rouse model with inertia in the continuum limit where the distances in the equations of motion are replaced by derivatives with respect to n can be found in ref. [37]. However, in this work we want to keep the discrete nature of the chain to obtain a better comparability with the expressions for the (free) harmonic chains.

First, we note that the reversible parts of the equations of motion are just the equations of motion for a free harmonic chain. Thus, using the same discrete cosine transforms as before (cf. eqs. (40) and (41)), we obtain the equations of motion for the modes

$$\dot{\tilde{q}}_n(t) = \frac{\tilde{p}_n(t)}{m}, \tag{58}$$

$$\dot{\tilde{p}}_n(t) = -m\Omega_n^2 \tilde{q}_n(t) - \gamma \tilde{p}_n(t) + \tilde{\xi}_n(t) \tag{59}$$

where $n \in \{0, \ldots, N-1\}$, Ω_n is the same as in eq. (45), and $\tilde{\xi}_n(t)$ is defined in exactly the same manner as the other transformed quantities.

These equations of motion are easily solved by standard textbook methods and the equilibrium-autocorrelation functions for the modes of the momentum read

$$\langle \tilde{p}_n(t)\tilde{p}_m(t')\rangle = \frac{b_n \delta_{nm}}{4\Omega_n^2 - \gamma^2}\left[\frac{\gamma\lambda_{n1} + 2\Omega_n^2}{2\gamma}\exp(\lambda_{n1}|t' - t|)\right.$$
$$\left. + \frac{\gamma\lambda_{n2} + 2\Omega_n^2}{2\gamma}\exp(\lambda_{n2}|t' - t|)\right] \tag{60}$$

where

$$\left\langle \tilde{\xi}_n(t)\tilde{\xi}_m(t')\right\rangle = \underbrace{2\gamma m k_B T(1 + \delta_{n0})}_{=:b_n}\delta_{nm}\delta(t - t'), \tag{61}$$

$$\lambda_{n1/2} := \frac{-\gamma \pm \sqrt{\gamma^2 - 4\Omega_n^2}}{2}. \tag{62}$$

We see that the autocorrelation function of the modes is either a sum of two exponential decays or an exponential decay multiplied with a sinusoid depending on the values of γ and Ω_n. In comparison one finds a simple exponential decay for the displacement modes in the usual Rouse model without inertia [38, 39] and stretched exponentials for entangled polymers [40]. The autocorrelation function for the momenta can now be expressed as

$$\langle p_n(t)p_n(t)\rangle = \frac{2}{N}\left(\frac{1}{4}\left\langle \tilde{p}_0(t)\tilde{p}_0(t')\right\rangle\right.$$
$$\left. + \sum_{i=1}^{N-1}\left\langle \tilde{p}_i(t)\tilde{p}_i(t')\right\rangle \cos^2\left(\frac{\pi i\left(n - \frac{1}{2}\right)}{N}\right)\right). \tag{63}$$

6 Results

6.1 Memory of Harmonic Chains in One Dimension

For a "chain" which consists only of one particle and two springs with fixed ends, we have only one mode and the velocity-correlation function reads

$$C_{\text{vel}}^{b}(t) = \frac{k_B T}{m}\cos\left(\sqrt{2}\omega t\right). \tag{64}$$

The Laplace transform of this is

$$\tilde{C}_{\text{vel}}^{b}(s) = \frac{k_B T}{m}\frac{s}{s^2 + 2\omega^2} \tag{65}$$

and the memory kernel reads (cf. (1,1) in table 1)

$$K_{\text{vel}}^{b}(t) = 2\omega^2. \tag{66}$$

Table 1 Memory kernels for the velocity of the n-th particle in a chain of length N with fixed ends

(N, n)	$K_{\text{vel}}^{\text{b}}(t)$
$(1, 1)$	$2\omega^2$
$(2, 1)$	$\frac{\omega^2}{2}\left(3 + \cos\left(\sqrt{2}\omega t\right)\right)$
$(3, 1)$	$\frac{\omega^2}{6}\left(8 + 3\cos(\omega t) + \cos\left(\sqrt{3}\omega t\right)\right)$
$(3, 2)$	$\omega^2\left(1 + \cos\left(\sqrt{2}\omega t\right)\right)$
$(4, 1)$	$\frac{\omega^2}{8}\left(10 + 2\cos\left(\sqrt{2}\omega t\right) + \right.$ $\left(2 + \sqrt{2}\right)\cos\left(\sqrt{2 - \sqrt{2}}\omega t\right) +$ $\left. \left(2 - \sqrt{2}\right)\cos\left(\sqrt{2 + \sqrt{2}}\omega t\right)\right)$
$(4, 2)$	$\frac{\omega^2}{6}\left(5 + 3\cos(\omega t) + 3\cos\left(\sqrt{2}\omega t\right) + \cos\left(\sqrt{3}\omega t\right)\right)$
$(5, 1)$	$\approx \omega^2(1.2 + 0.361804\cos(0.618034\omega t) +$ $0.261803\cos(1.17557\omega t) +$ $0.138197\cos(1.61803\omega t) +$ $0.0381966\cos(1.90211\omega t))$
$(5, 3)$	$\frac{\omega^2}{3}\left(2 + 3\cos(\omega t) + \cos\left(\sqrt{3}\omega t\right)\right)$
$(\infty, 1)$	$\omega^2 + \frac{\omega J_1(2\omega t)}{t}$

The interactions between the particles are purely harmonic and the systems are one dimensional. Due to the symmetry of the system, the memory kernels of the first and last particle of the chain, of the second and second to last particle of the chain, and so on, are identical. Hence, the memory kernel for, e.g., $(N, n) = (3, 1)$ is the same as the memory kernel for $(N, n) = (3, 3)$. For $(N, n) = (5, 1)$, the expression for the memory kernel contains roots of higher order polynomials that can either not be calculated exactly or have no concise representation. A numerical approximation of the coefficients in the expression of the memory kernel for the velocity of the first particle is given in the table

From the generalized Langevin equation

$$\frac{\mathrm{d}v(t)}{\mathrm{d}t} = -2\omega^2 \int_0^t \mathrm{d}\tau\, v(\tau) + \eta(t) \tag{67}$$

and the general time evolution of our observable $v(t) = \alpha \cos(\sqrt{2}\omega t + \phi)$ with constants α and ϕ, we see directly that the fluctuating force $\eta(t)$ has to be $\dot{v}(0)$ and that it does not explicitly depend on time. Further, the fluctuating forces are normally distributed because the initial velocities $v(0)$ are normally distributed in the canonical ensemble.

One can easily see that this memory kernel and these "fluctuating" forces (that do not fluctuate) fulfill the second fluctuation-kernel relation

$$\langle \eta(t)\eta(0)\rangle = K(t)\langle A(0)A(0)\rangle, \tag{68}$$

$$\langle \dot{v}(0)^2\rangle = 2\omega^2 \langle v(0)^2\rangle. \tag{69}$$

The same kind of analysis can be done for chains with more particles. However, as the calculations are more tedious, we use Wolfram Mathematica [41]. The resulting memory kernels for the chains with fixed ends are given in table 1 and the memory kernels for the

Table 2 Memory kernels for the velocity of the n-th particle in a chain of length N with free ends

(N, n)	$K_{\text{vel}}^{\text{f}}(t)$
(1, 1)	0
(2, 1)	$2\omega^2$
(3, 1)	$\frac{3\omega^2}{10}\left(4 + \cos\left(\sqrt{5/2}\omega t\right)\right)$
(3, 2)	$3\omega^2$
(4, 1)	$\frac{\omega^2}{21\sqrt{7}}\left(18\sqrt{7} + (7 + 5\sqrt{7})\cos\left(\sqrt{(7-\sqrt{7})/3}\omega t\right) - (7 - 5\sqrt{7})\cos\left(\sqrt{(7+\sqrt{7})/3}\omega t\right)\right)$
(4, 2)	$\approx \omega^2\left(2 + 0.459321\cos(0.885861\omega t) + 0.207345\cos(1.59643\omega t)\right)$
(5, 1)	$\approx \omega^2\left(\frac{2}{3} + 0.341775\cos(0.961264\omega t) + 0.18826\cos(1.51844\omega t) + 0.0532984\cos(1.87625\omega t)\right)$
(5, 2)	$\approx \omega^2\left(\frac{4}{3} + 0.908248\cos(0.880486\omega t) + \frac{1}{6}\cos(1.22474\omega t) + 0.0917517\cos(1.79576\omega t)\right)$
(5, 3)	$\frac{\omega^2}{2}\left(4 + \cos\left(\sqrt{5/2}\omega t\right)\right)$
(6, 1)	$\approx \omega^2(0.545455 + 0.305955\cos(0.796551\omega t) + 0.211176\cos(1.29501\omega t) + 0.108068\cos(1.67668\omega t) + 0.0293461\cos(1.9176\omega t))$

The interactions between the particles are purely harmonic and the systems are one dimensional. Due to the symmetry of the system, the memory kernels of the first and last particle of the chain, of the second and second to last particle of the chain, and so on, are identical. Hence, the memory kernel for, e.g., $(N, n) = (3, 1)$ is the same as the memory kernel for $(N, n) = (3, 3)$. For $(N, n) \in \{(4, 2), (5, 1), (5, 2), (6, 1)\}$, the expressions for the memory kernel contain roots of higher order polynomials that can either not be calculated exactly or have no concise representation. A numerical approximation of the coefficients in the expression of the memory kernel for the velocity of the first particle is given in the table

Table 3 Memory kernels for the displacement of the n-th particle in a chain of length N with fixed ends

(N, n)	$K_{dis}^b(t)$
$(1, 1)$	$2\omega^2$
$(2, 1)$	$\frac{3\omega^2}{10}\left(4+\cos(\sqrt{5/2}\omega t)\right)$
$(3, 1)$	$\frac{\omega^2}{21\sqrt{7}}\left(18\sqrt{7}+(7+5\sqrt{7})\cos\left(\sqrt{(7-\sqrt{7})/3}\omega t\right)-(7-5\sqrt{7})\cos\left(\sqrt{(7+\sqrt{7})/3}\omega t\right)\right)$
$(3, 2)$	$\frac{\omega^2}{3}\left(2+\cos\left(\sqrt{3}\omega t\right)\right)$
$(4, 1)$	$\approx \omega^2\left(\frac{2}{3}+0.341775\cos(0.961264\omega t)+0.18826\cos(1.51844\omega t)+0.0532984\cos(1.87625\omega t)\right)$
$(4, 2)$	$\frac{\omega^2}{78}\left(36+9\cos(\sqrt{5/2}\omega t)+(10-\sqrt{10})\cos\left(\sqrt{(7-\sqrt{10})/3}\omega t\right)+(10+\sqrt{10})\cos\left(\sqrt{(7+\sqrt{10})/3}\omega t\right)\right)$
$(5, 1)$	$\approx \omega^2(0.545455+0.305955\cos(0.796551\omega t)+0.211176\cos(1.29501\omega t)+0.108068\cos(1.67668\omega t)+0.0293461\cos(1.9176\omega t))$

The interactions between the particles are purely harmonic and the systems are one dimensional. Due to the symmetry of the system, the memory kernels of the first and last particle of the chain, of the second and second to last particle of the chain, and so on, are identical. Hence, the memory kernel for, e.g., $(N, n) = (3, 1)$ is the same as the memory kernel for $(N, n) = (3, 3)$. For $(N, n) \in \{(4, 1), (5, 1)\}$, the expressions for the memory kernel contain roots of higher order polynomials that can either not be calculated exactly or have no concise representation. A numerical approximation of the coefficients in the expression of the memory kernel for the velocity of the first particle is given in the table

velocity of the first particle in a free harmonic chain measured in the center-of-mass system are given in table 2.

To illustrate how an explicit expression for the fluctuating force can be derived for longer chains, we analyse the velocity of a particle in a chain of length two with fixed ends. In this case the memory kernel reads

$$K_{vel}^b(t) = \frac{\omega^2}{2}\left(3 + \cos(\sqrt{2}\omega t)\right) \tag{70}$$

and the velocity as a function of time reads

$$v(t) = \frac{1}{\sqrt{2m}}\Big[\tilde{p}_1(0)\cos(\omega t) - \tilde{q}_1(0)\omega\sin(\omega t)$$
$$+ \tilde{p}_2(0)\cos\left(\sqrt{3}\omega t\right) - \tilde{q}_2(0)\sqrt{3}\omega\sin(\sqrt{3}\omega t)\Big], \tag{71}$$

where $\tilde{p}_1(0), \tilde{q}_1(0), \tilde{p}_2(0), \tilde{q}_2(0)$ are randomly drawn from the initial canonical distribution. Now, we can calculate an expression for the fluctuating force via

$$\eta(t) = \dot{v}(t) + \int_0^t d\tau \, K_{vel}^b(t - \tau)v(\tau) \tag{72}$$

$$= \frac{\omega}{\sqrt{8m}}\Big[\omega\cos\left(\sqrt{2}\omega t\right)(\tilde{q}_1(0) - 3\tilde{q}_2(0))$$
$$- 3\omega\left(\tilde{q}_1(0) + \tilde{q}_2(0)\right)$$
$$+ \sqrt{2}\sin\left(\sqrt{2}\omega t\right)(\tilde{p}_1(0) - \tilde{p}_2(0))\Big]. \tag{73}$$

Let $\mathcal{N}(\mu, \sigma^2)$ denote a normal distribution with mean μ and variance σ^2. The distributions for the initial values in a canonical ensemble are given by

$$\tilde{q}_i(0) \sim \mathcal{N}\left(0, \frac{1}{\beta\Omega_i^2}\right), \tag{74}$$

$$\tilde{p}_i(0) \sim \mathcal{N}\left(0, \frac{1}{\beta}\right). \tag{75}$$

Hence, the distribution of the entire fluctuating force reads

$$\eta(t) \sim \mathcal{N}\left(0, \frac{2\omega^2}{\beta m}\right), \tag{76}$$

which is in perfect agreement with the fluctuation-kernel theorem. Further, we can see that the fluctuating force is also normally distributed for chains of arbitrary length with and without fixed ends. This follows immediately from the structure of the observable as a function in time, which is a sum of normally distributed starting configurations (with mean zero) multiplied with functions that depend solely on time (cf. for example eqs. (19), (20), (25) and (26) or the corresponding equations for the free chain). Consequently, the derivatives of these functions have the same structure and even the convolution with the memory kernel does not alter this structure. Thus, the fluctuating force has to be a normally distributed quantity. From the second fluctuation-kernel theorem we know the second moment of the fluctuating forces and, hence, we know the entire distribution.

Turning our focus back to the memory kernels, we see in fig. 2 that the memory kernels for the velocity of the first particle in finite chains with fixed ends agree with the memory
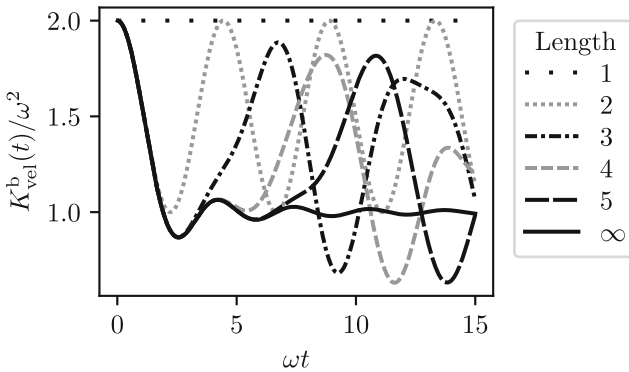
Fig. 2 Comparison of the memory kernels for the velocity of the first particle in chains with fixed ends and different lengths. The interactions between the particles are purely harmonic and the system is one dimensional
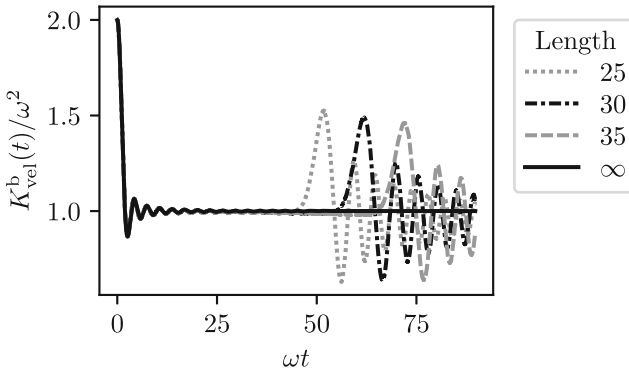
Fig. 3 Comparison of the memory kernels for the velocity of the first particle in chains with fixed ends and different lengths. The interactions between the particles are purely harmonic and the system is one dimensional. Here, the memory kernels for the finite lengths are obtained via a numerical scheme similar to the one introduced in ref. [23]. We see strong deviations between the memory kernels for chains of finite length and the one for the infinite chain starting around $\omega t \approx 2N$

kernel for the infinite chain over different periods in time. In general we can see that the times in which the memory kernels for the finite and infinite chain agree with one another increase roughly linearly with chain length. Numerical data for longer chains also agrees with this observation (compare fig. 3). This might suggest that the deviations of the memory kernels for finite chains from the one for the infinite chain stem from information that travels down the chain and returns after being reflected at the fixed end far away from the particle of interest.

Further, we notice that none of the memory kernels decay to zero for $t \to \infty$. The memory kernel for the infinite chain even converges $K_{vel}^b(t) \to \omega^2$ for $t \to \infty$. At this point we already want to point out that an increasing length of the chain leads to "less" structure in the memory kernel in the sense that $K_{vel}^b(t) \approx \omega^2$ for a longer duration after the initial "relaxation".

Next, we consider the memory kernels for the displacement instead of the velocity. Following the same procedure as before, one can derive some (quasi-)analytical results for short chains (see table 3). Comparing the expressions of the memory kernel for the velocity and

the displacement for chains of length $N = 2$

$$K_{\text{vel}}^{\text{b}}(t) = \frac{\omega^2}{2}\left(3 + \cos\left(\sqrt{2}\omega t\right)\right) \tag{77}$$

$$K_{\text{dis}}^{\text{b}}(t) = \frac{3\omega^2}{10}\left(4 + \cos\left(\sqrt{5/2}\omega t\right)\right) \tag{78}$$

we see that not even the frequencies of the first modes ($\sqrt{2}\omega$ and $\sqrt{5/2}\omega$) match up. Even though the dynamics are very simple in this case and one observable is the time-derivative of the other, it seems that there is no trivial relation between the memory kernels of the two observables.

(However, if one compares the memory kernels for the velocity of the first particle in a free chain of length N (cf. table 2) with the memory kernels for the displacement of the first particle in chains with fixed ends of length $N - 1$ (cf. table 3) one finds a perfect agreement. Using the expressions for the correlation functions, it is trivial to prove the equality for arbitrary lengths. This connection might very well be a mere coincidence and bear no physical insight.) Coming back to the displacement and velocity of a particle in a chain with fixed ends, one can also nicely illustrate that the Generalized Langevin equations for those quantities are not simply related by a time-derivative even though the observables are. We can calculate the derivative of the generalized Langevin equation for the displacement and perform an integration by parts to obtain an alternative equation of motion for the velocity:

$$\ddot{q}(t) = -\frac{\mathrm{d}}{\mathrm{d}t}\int_0^t \mathrm{d}\tau\, K_{\text{dis}}^{\text{b}}(t - \tau)q(\tau) + \dot{\eta}(t), \tag{79}$$

$$\dot{v}(t) = -\int_0^t \mathrm{d}\tau\, K_{\text{dis}}^{\text{b}}(t - \tau)v(\tau) - K_{\text{dis}}(t)q(0) + \dot{\eta}(t). \tag{80}$$

Note that there is no fluctuation-kernel relation between $K_{\text{dis}}^{\text{b}}(t)$ and $\dot{\eta}(t)$. Thus the memory kernel of the equation of motion for the velocity that is derived directly by a linear projector (and thus fulfills eq. 8 by construction) has to differ from $K_{\text{dis}}^{\text{b}}(t)$.

The correlations of the displacement in an infinite chain with fixed ends are more complicated than the correlations of the velocity in an infinite chain with fixed ends. Hence, we use the numerical result for the memory kernel for a long chain (500 particles) as a reference in fig. 4. Besides the obvious similarities between the memory kernels for the velocity and the displacement (e.g. the number of modes or the expression $K_{\text{dis/vel}}^{\text{b}}(t) = 2\omega^2$ for a chain of length one), there are some striking differences. For example, the convergence with increasing chain length is much slower than for the velocities (see also fig. 5), and the value of the memory kernel at $t = 0$ depends on the length of the chain. Both of these findings may be explained by the fact that the equilibrium probability distribution for the displacements depends on the length of the chain. In contrast to this, the probability distribution of the velocities is normal ($p(v) \sim \exp(-\beta m v^2/2)$) irrespective of the length of the chain. Another remarkable difference is that the memory kernel for the displacement of the first particle in an infinite chain seems to decay to zero for large times whereas the memory kernel for the velocity of the first particle in an infinite chain decays to ω^2 for large times.

However, there is another case in which the memory kernel decays to zero even when we consider the velocity as the observable of interest. The expression for the infinite chain derived above corresponds to the case of only one fixed end as the second fixed end is pushed towards infinity when the thermodynamic limit is taken. If we want to eliminate the effect of
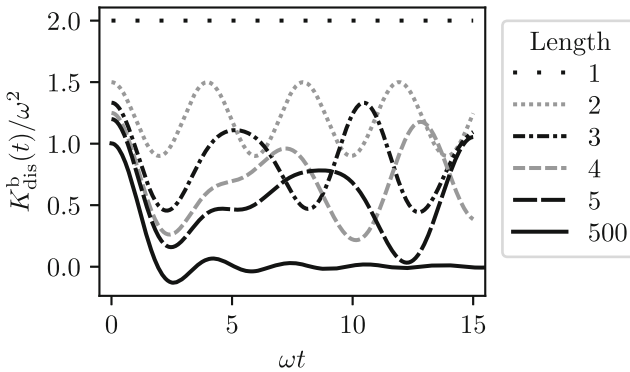
Fig. 4 Comparison of the memory kernels for the displacement of the first particle in chains with fixed ends and different lengths. The interactions between the particles are purely harmonic and the system is one dimensional. The first five memory kernels are obtained via the method involving a Laplace transform, the memory kernel for a length of 500 is obtained via the method described in ref. [23]

any hard wall, we can study the dynamics of a particle in the infinite chain, which is also far away from the first fixed end. We first notice that for any fixed $\omega > 0$ and $\forall t \in \mathbb{R}$

$$\lim_{j \to \infty} J_{4j}(2\omega t) \to 0 \tag{81}$$

in eq. (38). Thus, we conclude that the velocity covariance for the infinite chain (extending infinitely in both directions) with no fixed ends reads

$$C_{\text{vel}}^{\text{f}}(t) = \frac{k_{\text{B}} T}{m} J_0(2\omega t) \tag{82}$$

which agrees with the result for an infinite chain with periodic boundary conditions in ref. [29]. Calculating the memory kernel from this expression one obtains

$$K_{\text{vel}}^{\text{f}}(t) = \frac{2\omega J_1(2\omega t)}{t}. \tag{83}$$

This differs from all previous memory kernels for velocities as this memory kernel vanishes for $t \to \infty$. In ref. [29] it is found that the velocity covariance in eq. (82) gives rise to a nonzero diffusion coefficient due to its zero-frequency mode. In order to obtain a diffusive process, however, it is sensible that the particle "forgets about its past" at some point during the process.

6.2 Introducing Anharmonicities

There are many different ways to introduce anharmonicities in the interaction potential. One way is to replace the quadratic interaction by a potential which is a polynomial of order four as done in ref. [42]. There, the relevant time scales of the intermediate scattering functions and their memory kernels show a sensitive dependency on the strength of the anharmonicity.

For the systems studied in this work, if not stated otherwise, we use a harmonic interaction that is equivalent with the harmonic limit in ref. [42]. In particular we use a spring coefficient of $k = 20.14\beta^{-1}d^{-2}$ where d is the equilibrium distance. However, the anharmonicity introduced in ref. [42] seems not to be the intuitive one if one thinks about modeling polymers.
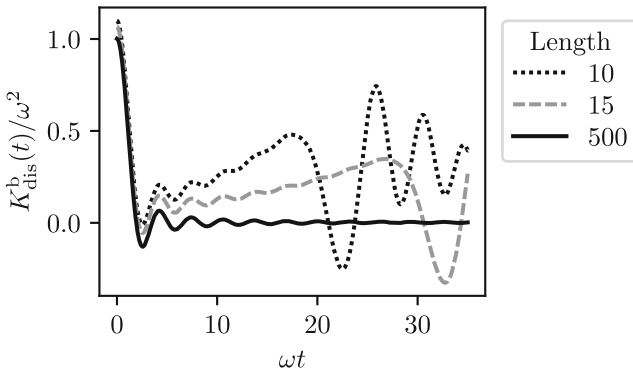
Fig. 5 Comparison of the memory kernels for the displacement of the first particle in chains with fixed ends and different lengths. The interactions between the particles are purely harmonic and the system is one dimensional. All memory kernels are obtained via the method described in ref. [23]
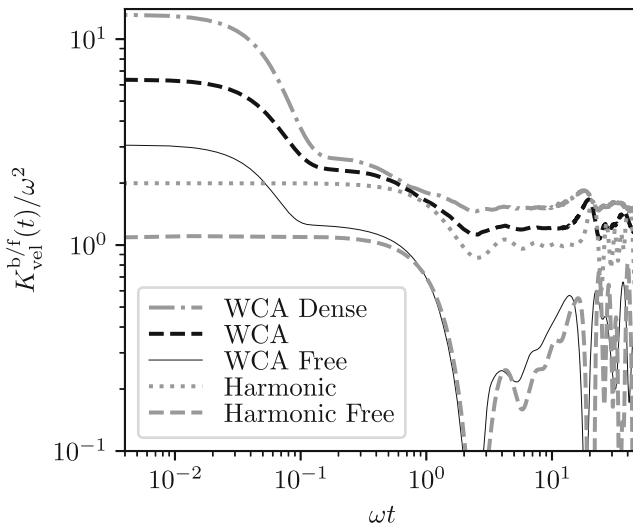

Fig. 6 Memory kernels for the velocity of the first particle in a chain of length 10. All systems are one dimensional. The "Harmonic" and "Harmonic Free" curves have purely harmonic interactions, whereas the "WCA", "WCA Dense", and "WCA Free" curves include a WCA interaction to model the steric interactions among the particles. The equilibrium distance of neighbouring particles for the "WCA" and "WCA Free" curves are $\Delta x = 1$ and for the "WCA Dense" curve it is $\Delta x = 0.9$. For the "Harmonic Free" and "WCA Free" curves no fixed ends are used

Instead we add a Weeks-Chandler-Andersen (WCA) interaction among the particles to model steric interactions. The expression for the WCA potential [43] reads:

$$V_{\mathrm{WCA}}(r) = \begin{cases} 4\epsilon \left(\left(\frac{\sigma}{r} \right)^{12} - \left(\frac{\sigma}{r} \right)^{6} \right) + \epsilon & \text{for } r \leq r_{\mathrm{co}} \\ 0 & \text{for } r > r_{\mathrm{co}} \end{cases} \qquad (84)$$

with the cut-off radius $r_{\mathrm{co}} = 2^{1/6}\sigma$. For now, we use $r_{\mathrm{co}} = 0.6d$ and $\epsilon = 20\beta^{-1}$.

For a start, we run two sets of simulations each with ten particles but one with a distance of $l = 11d$ and one with a distance of $l = 9.9d$ between the walls. These correspond to
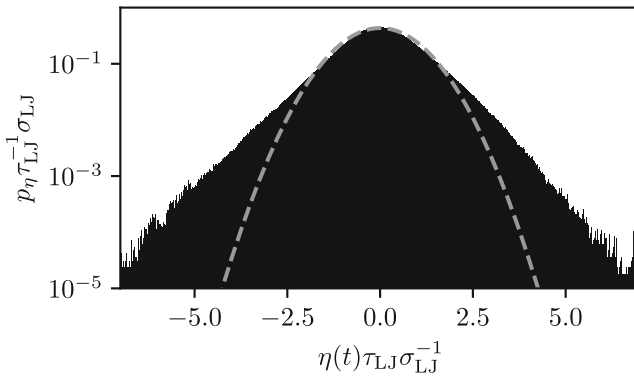
Fig. 7 Distribution of the fluctuating force of the generalized Langevin equation for the displacement of one particle in a one dimensional chain with fixed ends and a WCA interaction. For comparison, a fitted normal distribution is also depicted. The distribution has been obtained by rescaling the histogram and the only fit parameter for the normal distribution is the standard deviation

equilibrium distances between neighbouring particles of either $\Delta x = 1d$ or $\Delta x = 0.9d$. By decreasing Δx we can increase the number of "WCA collisions" taking place and, thus, investigate the influence of the number of collisions on the memory kernels. From the velocity covariance we calculate the memory kernels shown in fig. 6. For both sets of simulations the average duration of a "WCA collision" is determined to be around $\omega\Delta t \approx 0.1$ which is in perfect agreement with the peaks in the memory kernels for the "WCA" and "WCA Dense" curves at $\omega t = 0$. Interestingly, one does not see a clear signature of the WCA interaction on the time scale of the collisions for the autocorrelation functions that yield these memory kernels (c.f. Appendix 1). For times $\omega t > 0.1$ the curves including WCA interactions lay slightly above the purely harmonic ones but exhibit similar behavior (e.g. after $\omega t \approx 20$ the memory kernel shows again some stronger oscillations). The average number of collisions per time for the "WCA" setup is $N_{col}/T \approx 2.5$ and for the "WCA Dense" setup it is $N_{col}/T \approx 5.6$. The ratio of these collision rates is similar to the ratio of the heights of the peaks of the memory kernels at $\omega t = 0$. Thus, one might expect to see an even stronger peak in systems with more collisions such as a polymer melt in three dimensions.

Next we analyse the distribution of the fluctuating forces for this system. We can use eq. (10) together with the memory kernels we determined above and the MD trajectories to calculate the fluctuating forces via

$$\eta(t) = \frac{dA(t)}{dt} + \int_0^t d\tau \, K(t-\tau)A(\tau). \tag{85}$$

In fig. 7 an exemplary distribution for the displacement is shown. The distribution for the velocity looks quite similar and is hence omitted. As one can see, the fit of a normal distribution in fig. 7 does not match the real distribution at all and, hence, one should not approximate the random force for such a system by Gaussian noise. A similar result was found by analyzing the fluctuating forces for a simple diffusion process where a Gaussian noise distribution is recovered for heavy tracer particles only [27]. In more general terms we want to emphasize that a non-trivial memory kernel does not imply a non-Gaussian distribution of the fluctuating forces. Instead, one can always find a random process with a Gaussian distribution that satisfies the fluctuation-kernel relation, eq. (8), and reproduces the autocorrelation functions
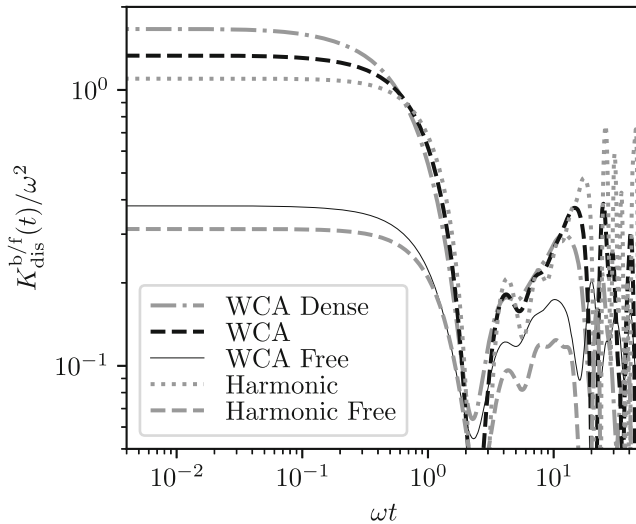
Fig. 8 Memory kernels for the displacement of the first particle in a chain of length 10. All system are one dimensional. The "Harmonic" and "Harmonic Free" curves have purely harmonic interactions, whereas the "WCA", "WCA Dense", and "WCA Free" curves include a WCA interaction to model the steric interactions among the particles. The equilibrium distance of neighbouring particles for the "WCA" and "WCA Free" curves are $\Delta x = 1$ and for the "WCA Dense" curve it is $\Delta x = 0.9$. For the "Harmonic Free" and "WCA Free" curves no fixed ends are used

of the observables exactly. This is true for stationary processes [44] as well as for non-stationary processes [24]. However, the fluctuating forces are then not modeled via white Gaussian noise but drawn from a multidimensional Gaussian distribution.

Now, we look into the dynamics of the velocity of the first particle in a chain with no fixed ends (see "WCA Free" in fig. 6). If we show memory kernels for observables of free polymers, these are always sampled in the center of mass system and shifted such that the time average of the observables vanishes. The shift is only important for the displacement since the time average of the velocity in the center of mass system is zero anyways.

For short times $\omega t < 1$, the memory kernels for "WCA" and "WCA Free" show similar trends but differ approximately by a factor of two. This is in agreement with the previous connections drawn between the structure of the memory kernels and the interactions because the first particle in the freely floating chain interacts only with one instead of two neighboring particles via a harmonic and a WCA interaction. For larger times, $\omega t > 0.1$, the memory kernels for the free polymers with and without a WCA interaction are similar, e.g. both are smaller in magnitude than the other memory kernels in fig. 6. However, it can be seen that the WCA interaction removes a considerable amount of structure from the memory kernel for late times (see for example the amplitude of the oscillations for $\omega t > 20$).

The memory kernels for the displacement can be seen in fig. 8. The main difference between the memory kernels for the velocity and the displacement, besides the points discussed before, is that there is no additional peak from the WCA interaction for the displacements. To understand why this is the case we use eq. (13) to get a first approximation of the memory kernel by the first term on the right-hand side:

$$K(t) \approx -\frac{\ddot{C}(t)}{C(0)}. \tag{86}$$
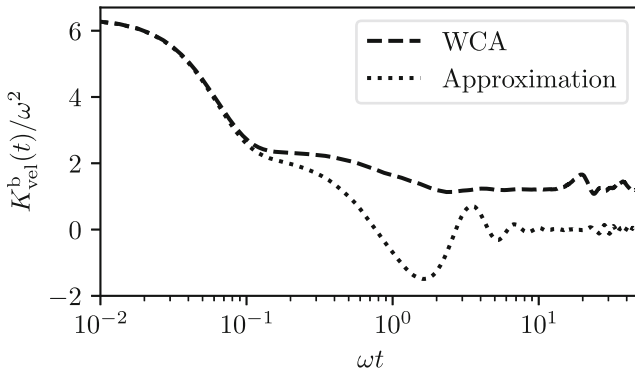
Fig. 9 Memory kernel and approximation of the memory kernel for the velocity of the first particle in a chain of length ten with fixed ends. The system is one dimensional and the individual particles in the chain interact via a harmonic and a WCA interaction. The explicit form of the approximation is given in eq. (86)
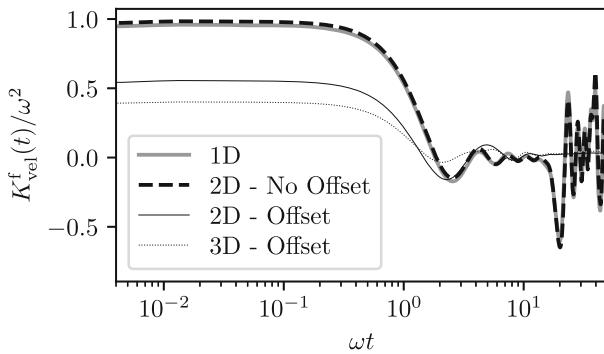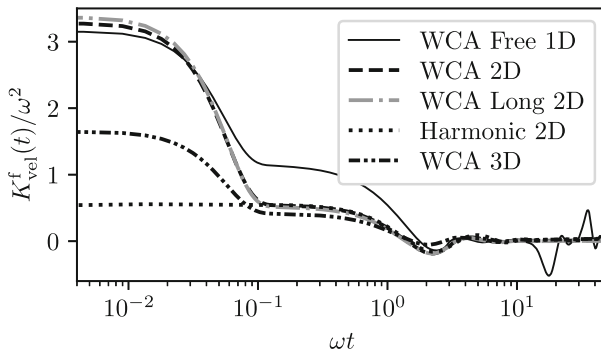

Fig. 10 Memory kernels for the velocity of the end particle in a free harmonic chain of length ten. The systems differ in their dimensionality going from one to three. For the "2D - Offset" and "3D - Offset" curves a offset of $r_0 = d$ in the interaction potential is picked

This corresponds to the so called $\mathcal{Q}$-approximation where the orthogonal evolution operator is replaced by the full time-evolution operator [15, 20, 45, 46]. If we use this to calculate an approximation of the memory kernel for the displacement, we obtain something proportional to the velocity correlation function, that does not show this peak around $t = 0$ due to the WCA interacton (cf. eq. (37)). On the other hand, if this approximation is used for the memory kernel of the velocity, we obtain

$$K_{\text{vel}}^{\text{b/f}}(t) \approx \frac{\langle F(0) F(t)\rangle}{m^2 \langle v(0)^2\rangle}. \tag{87}$$

Here, the force correlation and, hence, the peak due to the WCA interaction enters immediately. In fig. 9 the memory kernel for the velocity of a chain with WCA interaction is shown as well as the approximation discussed here. On the time scale of the WCA peak the approximation of the memory kernel fits the true memory kernel perfectly.

Fig. 11 Memory kernel for the velocity of the first particle in a chain of length ten, only the "WCA Long 2D" curve is for a chain of length twenty. All chains are free, meaning that they have no fixed ends. The dimensionality of the systems varies and goes from one up to three

6.3 Going to Higher Dimensions

If we look again at a chain with purely harmonic interactions, we will get the same results in two dimensions as in one dimension because the equations of motion for the different dimensions decouple (see fig. 10, the curves for "1D" and "2D - No Offset"). However, this is only true as long as the equilibrium distance of the springs is zero or in other words, only if we consider the interaction potential

$$V(r) = \frac{k}{2} (r - r_0)^2 \tag{88}$$

with $r_0 = 0$. Otherwise, the force acting on a particle in x-direction would depend on the distance in y-direction (through r)

$$F_x = -\partial_x V(r) = -k \left(x - \frac{r_0 x}{r} \right). \tag{89}$$

The effect of this coupling can be seen in fig. 10. Here, the "2D - Offset" and "3D - Offset" curves (with $r_0 = 1d$) have a less pronounced peak at $\omega t = 0$ and for $\omega t > 20$ there is no signal like the one in the "1D" or "2D - No Offset" cases. Note, that in "1D" r_0 has no effect on the dynamics.

With the WCA interaction, however, matters change in higher dimensions as now also particles that are not direct neighbors can interact via the WCA interaction. Comparing the memory kernels for the velocity labeled "WCA 2D" and "WCA Long 2D" in fig. 11 we see that the magnitude of the peak at $\omega t = 0$ slightly increases with the length of the chain. For times larger than the usual time of a collision ($\omega t \approx 0.1$) the WCA interaction seems not to affect the shape of the memory kernel at all as the offset in the harmonic interaction potential already removes the signal for $\omega t > 10$.

Interestingly, one can observe an opposite effect if one considers again the displacement as the observable (see fig. 12). Again, there is no initial peak on the timescale of the "WCA collisions". However, the initial peak on the time scale of the harmonic oscillations gets less pronounced with the onset of the "WCA" interaction and gets even smaller for increasing chain lengths. An intuitive explanation for this is that for the velocities the WCA interactions cause rapid changes of the value of the observable. For the displacements, on the other hand, the WCA interaction can "lock" the value of the observable as other particles may be regarded
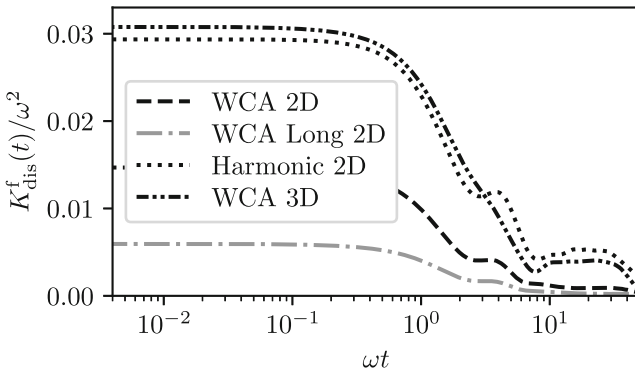
Fig. 12 Memory kernel for the displacement of the first particle in a chain of length ten, only the "WCA Long 2D" curve is for a chain of length twenty. All chains are free, meaning that they have no fixed ends. All systems are either two or three dimensional
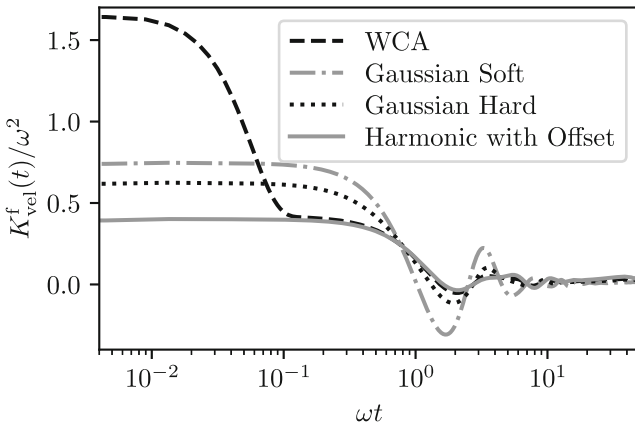

Fig. 13 Memory kernels for the velocity of the first particle in a chain of length ten. All systems are three dimensional. The additional anharmonicities of the chain are either a WCA interaction or a Gaussian ineraction. For the "Harmonic with Offset" curve a offset of $r_0 = d$ is picked

as barricades that slow down the dynamics of the displacement. This also explains why the "WCA 3D" curve has a less pronounced peak than the "WCA 2D" curve for the velocities (see fig. 11) but a stronger one for the displacements (see fig. 12). In three dimensions the particles can go round each other more easily and collide less. This argument is further strengthened by the fact that the displacement-autocorrelation function in three dimensions decays faster than in two dimensions (c.f. Appendix 1).

Next we want to illustrate that the general trends observed in this section are not just a result of the specific anharmonicity we chose, the WCA interaction. In fig. 13 memory kernels for the velocity of chains in three dimensions can be seen. For two of them a Gaussian interaction potential of the form

$$V_{\text{Gaussian}}(r) = \epsilon \exp\left(-\frac{1}{2}\left(\frac{r}{\sigma}\right)^2\right) \tag{90}$$

is used instead of the WCA interaction. The Gaussian interaction model is capable of reproducing important properties of polymer systems, e. g. depletion interactions [47]. For
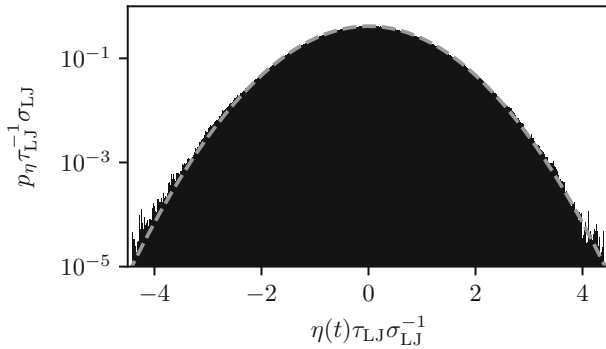
Fig. 14 Distribution of the fluctuating force of the generalized Langevin equation for the displacement of the first particle in a chain without fixed ends in two dimensions. The interaction potential is purely harmonic with a nonzero offset. For comparison a fitted normal distribution is depicted. The distribution has been obtained by rescaling the histogram and the only fit parameter for the normal distribution is the standard deviation
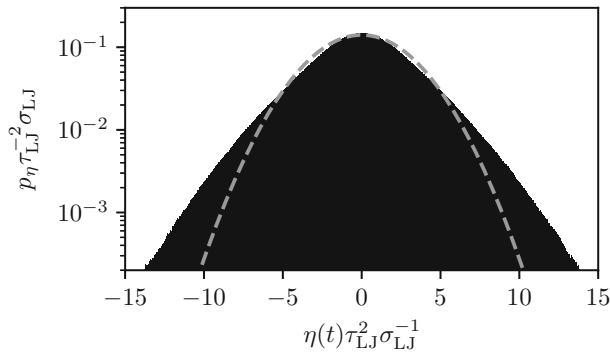

Fig. 15 Distribution of the fluctuating force of the generalized Langevin equation for the velocity of the first particle in a chain without fixed ends in two dimensions. The interaction potential is purely harmonic with a nonzero offset. For comparison a fitted normal distribution is depicted. The distribution has been obtained by rescaling the histogram and the only fit parameter for the normal distribution is the standard deviation

simplicity we pick the same values for ϵ and σ as used for the WCA interaction (cf. eq. (84)). The corresponding curve in fig. 13 is labeled "Gaussian Soft". For the "Gaussian Hard" curve ϵ is doubled and σ is halved. We can see that the overall timescale of the decay of the memory is quite similar for all interactions. However, only for the WCA interaction we can clearly attribute the different signatures of the memory kernel to the different kinds of interactions, e.g. the initial peak at $\omega t = 0$ to the WCA interaction and the decay around $\omega t = 1$ to the harmonic one. For the Gaussian interaction, which has no cutoff radius here, the different interactions interfere more which each other and one cannot differentiate between their effects as clearly as with the WCA interaction.

Finally, we analyse the distributions of the fluctuating forces of the two-dimensional systems. Interestingly the hard interaction has no strong effect on the shape of the distributions and hence we restrict ourselves to showing only the data for the purely harmonic case with an offset. Again, the distributions obtained from the simulations are shown together with fitted normal distributions, fig. 14 for the displacement and in fig. 15 for the velocity. Interestingly, the distribution of the fluctuating forces for the displacement can be well described with a
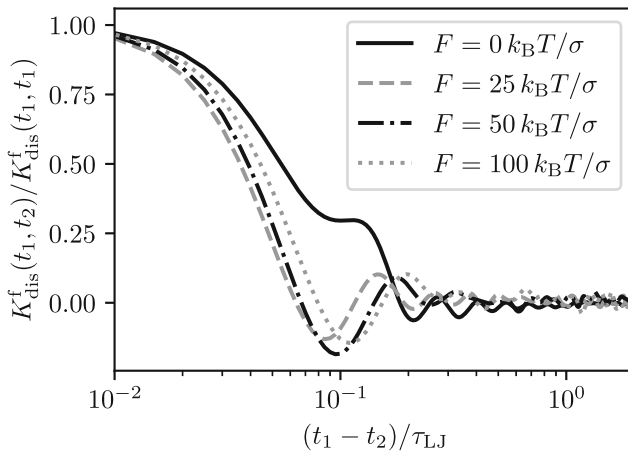
Fig. 16 Normalized memory kernels for the displacement of the last particle in a polymer where an external force acts on the first particle of the same polymer within a polymer melt. All systems are three dimensional. The memory kernels are shown for $t_1 = 10\tau_{LJ}$

normal distribution whereas this is not the case for the distribution of the fluctuating forces for the velocity.

### 6.4 Melts and Non-equilibrium

Next, we address full non-equilibrium systems. We study a polymer melt and apply an external force to one particle in one polymer from the melt. We choose the displacement (e.g. $\Delta x(t) = x(t) - x(0)$) as the observable of interest. Even though this observable is similar to the previous observables, the formalism to derive an equation of motion changes considerably, because the displacement of the particles (in free space) does not reach a stationary distribution. In other words, the two-time correlation function $C(t_1, t_2) := \langle \Delta x(t_1) \, \Delta x(t_2) \rangle$ is not invariant under time translations $C(t_1, t_2) \neq C(t_1 + \Delta t, t_2 + \Delta t)$. Hence, even without an external force the dynamics cannot be described by the stationary generalized Langevin equation (eq. (10)) but needs to be described by the non-stationary generalized Langevin equation (eq. (1)).

We perform molecular dynamics simulations of Kremer–Grest bead-spring polymer melts [48] at a monomer density of $n\sigma^3 = 0.85$. Our simulations consist of $N_{ch} = 125$ chains of $N = 100$ monomers each, i.e. of $N_{ch}N = 12,500$ particles. Each monomer has a mass m and interacts through the Weeks-Chandler-Andersen (WCA) potential, eq. (84), with $\epsilon = k_B T$, leading to a time scale $\tau_{LJ} = \sqrt{(m\sigma^2)/\epsilon}$. Covalent bonds are modeled using a non-linear elastic potential (FENE),

$$U_{FENE}(r) = -(k_{FENE} R_0^2/2) \ln \left(1 - (r/R_0)^2\right), \tag{91}$$

with $k_{FENE} = 30\epsilon/\sigma^2$ and $R_0 = 1.5\sigma$. The simulations are carried out in a cubic box using periodic boundary conditions. A constant external force F_{ext} is applied along the positive x-direction on the first monomer of a tracer polymer chain. To obtain statistically significant results, we simulate at least 1.6×10^3 independent trajectories for each data set.

The memory kernels for displacement and velocity at different external force strengths are shown in figs. 16 and 17. Some exemplary 3D plots of two-time correlation functions as
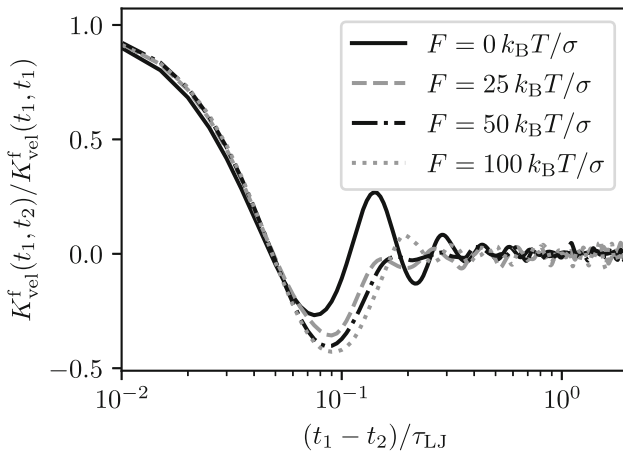
Fig. 17 Normalized memory kernels for the velocity of the last particle in a polymer where an external force acts on the first particle of the same polymer within a polymer melt. All systems are three dimensional. The memory kernels are shown for $t_1 = 10\tau_{LJ}$
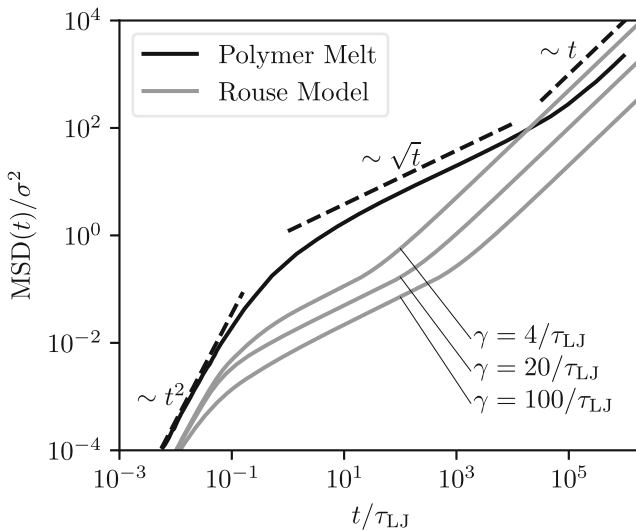
Fig. 18 Mean square displacement (MSD) of the end monomers in polymer chains of length $N = 100$. The black curve is obtained from equilibrium simulations of a polymer melt and the grey curves are the analytic MSD's for the Rouse chain with inertia for three different friction constants. For all curves one can see a ballistic regime ($\sim t^2$) at short times, a subdiffusive regime ($\sim \sqrt{t}$) at intermediate times, and a diffusive regime ($\sim t$) at late times

well as memory kernels reflecting the non-stationary nature of the problem are shown and discussed in Appendix 2. Similar to our previous results, we see that the memory kernels decay rapidly, with some minor variations depending on the external force. However, the overall decay behavior remains mostly unaffected. For the simpler systems discussed earlier, this decay occurs on a time scale of ω^{-1}. To analyze these systems in a similar fashion, we determine an effective spring constant considering the second derivative of the interaction

potential (WCA+FENE) at its minimum. This analysis yields $k_{eff} \approx \sqrt{981.255} \frac{\epsilon}{\sigma^2}$, which in turn results in $\omega_{eff} = \sqrt{\frac{k_{eff}}{m}} \approx 31.32 \tau_{LJ}^{-1}$. The time scale $\omega_{eff}^{-1} \approx 0.032 \tau_{LJ}$ fits the decay time scale of the memory kernels nicely. Furthermore, we observe some common features of the memory kernels for the same observables among the different systems. For example, the memory kernels for the displacement in the case of a free chain in two dimensions (fig. 12) and the memory kernel for the displacement in a polymer melt without an external force (fig. 16) exhibit a similar non-monotonic behaviour during the initial decay.

If we consider the mean square displacement (cf. fig. 18), we see a clear subdiffusive regime for the polymer melt. Here, it starts around the time a monomer needs to traverse its own diameter, $\text{MSD}(t) = \sigma^2$, which is $t \approx 3.5 \tau_{LJ}$ and extends to times of the order of $10^5 \tau_{LJ}$. With a chain length of $N = 100$ one might expect to see first hints of reptation, e.g. a regime in the MSD with $\text{MSD}(t) \sim t^{1/4}$. However, as shown in ref. [48], this effect is strongly suppressed for monomers close to the ends of the polymers because their movement is less constrained than the movement of monomers close to the center of the polymers. Thus, it is not surprising that we do not observe a repation regime here.

To get a better understanding of the subdiffusive signature, we compare it with the MSD of the Rouse model with inertia. The MSD for the Rouse model is easily obtained by dividing the momentum-autocorrelation function, eq. (63), by m^2 and integrating it over time twice. In the resulting expression, we use a chain length of $N = 100$ and a spring constant of $k = 31.32 k_B T \sigma^{-2}$ in direct analogy to the polymer-melt system. We show the MSDs for three different different values of the friction constant $\gamma \tau_{LJ} \in \{4, 20, 100\}$ in fig. 18. While the different MSDs qualitatively reproduce the MSD of the polymer melt in the sense that they show a ballistic, a subdiffusive, and a diffusive regime, they do not agree quantitatively. This might be expected from all the simplifications in the Rouse model. However, we see that a friction constant $4 < \gamma \tau_{LJ} < 20$ will reproduce the correct long-time diffusion constant while larger friction constants better reproduce the extent of the subdiffusive regime.

Next, we check how this behaviour is entailed in the memory kernels. For very short chains, the memory kernels can be calculated analytically via eq. (12). The memory kernel for the velocity of a particle in a Rouse chain with inertia of length two the memory kernel reads

$$K_{vel}^f(t) = \gamma \delta(t) + \omega^2 \exp\left(-\frac{\gamma t}{2}\right) \left[\cosh\left(\frac{\sqrt{\gamma^2 - 4\omega^2}}{2} t\right) \right.$$

$$\left. + \frac{\gamma}{\sqrt{\gamma^2 - 4\omega^2}} \sinh\left(\frac{\sqrt{\gamma^2 - 4\omega^2}}{2} t\right) \right]. \tag{92}$$

Here, the delta peak at $t = 0$ is a clear signature of the noise in the equations of motion. Further, we see that the memory kernel decays exponentially. We also determine the analytic memory kernels $K_{vel}^f(t)$ for chains up to a length of $N = 4$. However, the exact expressions are quite long and not very insightful. Thus, they are left out and we simply note that all of them have a delta-peak contribution of the form $\gamma \delta(t)$ and all the other terms are exponentially decaying. This nicely fits to findings of ref. [49] where it is shown that the memory kernel for the displacement of the central particle in a Rouse chain without inertia but in the continuum limit is a sum over infinitely many exponential decays.

The memory kernels for Rouse chains of length $N = 100$ are again calculated numerically. A comparison of the equilibrium memory kernels for the polymer melt and the Rouse model with different friction constant can be seen in fig. 19. Surprisingly, the memory kernel for the polymer melt seems to decay much faster than the memory kernels for the Rouse model even though the subdiffusive regime for the polymer melt extends to loger times than for the three
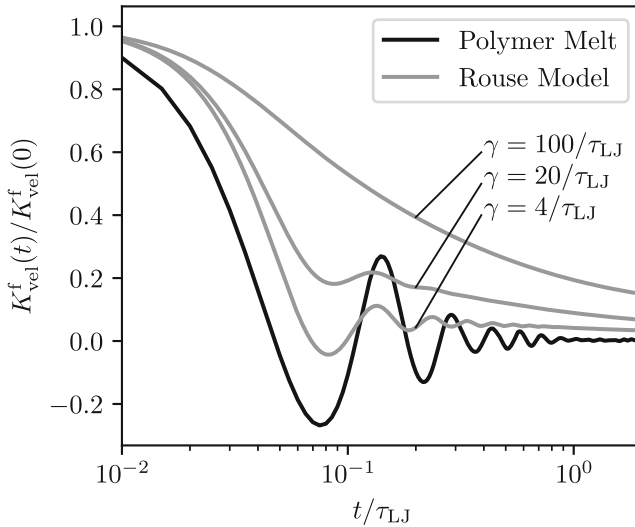
Fig. 19 Normalized memory kernels for the velocities of the end monomers in a polymer chain of length $N = 100$. The black curve is obtained from equilibrium simulations of a polymer melt and the grey curves are obtained by numerically calculating the memory kernels from the analytic expression of the velocity-autocorrelation function for the Rouse model with inertia and three different friction constants. Note that the delta-peak contribution is ignored for the normalization of the memory kernels for the Rouse model

depicted Rouse systems. However, it is possible that there are slower decaying contributions to the polymer-melt memory kernel that have such a small amplitude that they are buried in the noise. Here, one has to keep in mind that the normalization of the memory kernels in fig. 19 might give a misleading impression, because the $\gamma\delta(t)$ contribution to all memory kernels of the Rouse model is ignored for the normalization.

7 Conclusion

We have presented an analysis of the motion of a single particle in a one-dimensional chain. By means of the projection operator method we have integrated out the degrees of freedom of all other particles in order to obtain the effective equation of motion, the generalized Langevin equation. We started out with a harmonic chain in one dimension and successively increased the complexity of the problem by adding anharmonic interactions, considering higher dimensions and pulling on the particle. In particular, we were interested in the effects of these different levels of complexity on the memory kernel and the distribution of the fluctuating force.

Starting out from one-dimensional harmonic chains where the memory kernel never decays, it is shown that different sources of nonlinearities lead to quickly decaying memory kernels. (Note, that the framework of the generalized Langevin equation does not rely on any point throughout the derivation on the fact that the memory kernels decay to zero. Of course, a memory kernel that does not decay may complicate a stochastic interpretation of the fluctuating force and, thus, prevent us from using the generalized Langevin equation as a simple coarse-graines model. Nevertheless the formalism may still be useful to analyze such systems.)
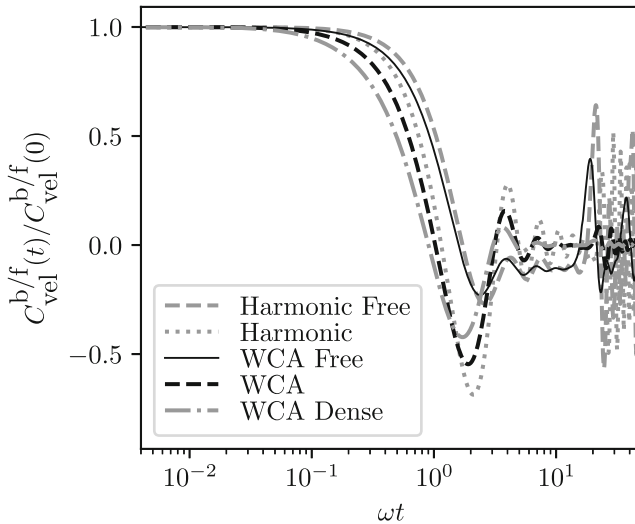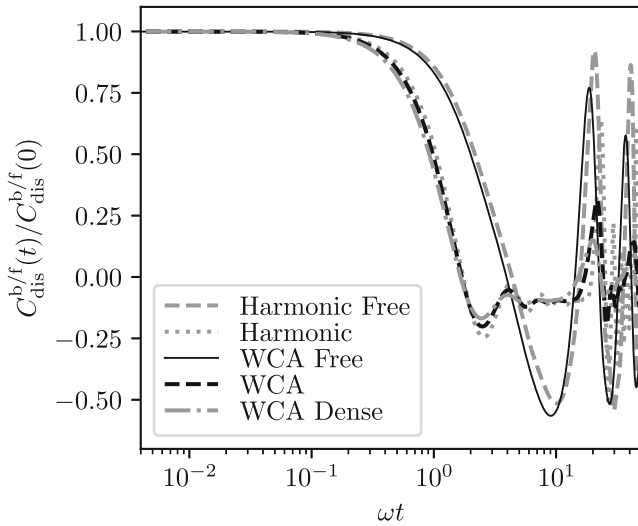
Fig. 20 Normalized velocity autocorrelation functions yielding the memory kernels in fig. 6. All systems are one dimensional

Introducing anharmonicities in the form of Weeks-Chandler-Anderson (WCA) interactions, for example, causes a decay of the memory kernels and gives rise to an additional peak in the memory kernel that can be associated with WCA collisions. Going to higher spacial dimensions also causes the memory kernel to rapidly decay if a nonzero equilibrium distance between the particles is chosen. Further, in many cases we analyzed, the fluctuating forces do not have a simple normal distribution. Thus, if one wishes to use a Langevin equation to model such systems, the noise should not be drawn from a normal distribution. Going to a system of anharmonically interacting chains in three dimensions, a simple polymer-melt model, a similar trend is observed. Here, the decay of the memory kernels of the end monomers in the polymer melt decays much faster at short times than the memory kernels obtained for a Rouse model with inertia. Further, an analysis of driven systems where a single polymer is pulled through the melt with a constant force shows that this rapid decay is also obtained in an adapted version of the generalized Langevin equation suitable for full non-equilibrium systems.

We conclude that the structured part of the memory kernel, which dominates the behaviour of the auto-correlation function at short times, vanishes for increasingly complex systems.

Appendix: Correlation Functions

In this appendix we show show a selection of correlation functions for the different models and observables considered throughout the article. The correlation functions in figs. 20, 21, 22, 23 lead to the memory kernels in figs. 6, 8, 11 and 12 respectively. Interestingly, the clear signal of the WCA interaction for the memory kernels of the velocity, the peak for $\omega t \lesssim 10^{-1}$,
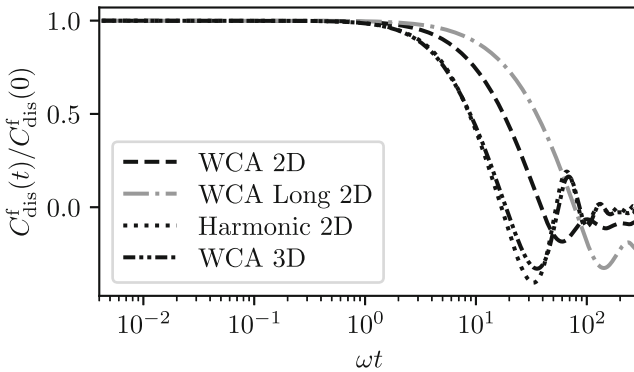
Fig. 21 Normalized displacement autocorrelation functions yielding the memory kernels in fig. 8. All systems are one dimensional
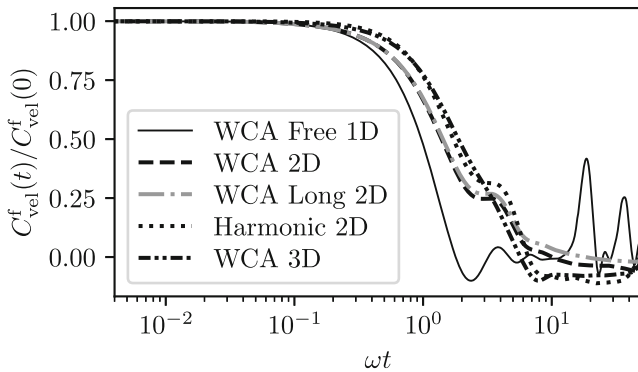
Fig. 22 Normalized velocity autocorrelation functions yielding the memory kernels in fig. 11. The dimensionality of the systems varies and goes from one up to three

is not visible in the corresponding velocity autocorrelation functions (c.f. figs. 20 and 22). Regarding the "WCA 2D" and "WCA 3D" curves in fig. 23, we find further evidence that the reasoning why the "WCA 3D" memory kernel has a less pronounced peak than the "WCA 2D" memory kernel in fig. 11, namely that in three dimensions the particles can go round each other more easily and collide less, is correct.

Fig. 23 Normalized displacement autocorrelation functions yielding the memory kernels in fig. 12. All systems are either two or three dimensional

## Non-stationary Correlation Functions and Memory Kernels

In this section we show some exemplary 3D plots of two-time correlation functions and memory kernels in the non-stationary case discussed in section 6.4. Because we want to discuss only the qualitative behaviour, we only show plots for an external force of $F = 50k_\mathrm{B}T/\sigma$ in this section. In figs. 24 and 25 the two-time correlation functions for the displacement and the velocity are shown. As expected, the two-time correlation function of the displacement does not reach a stationary limit but shows a steady increase with increasing t_1 and t_2. The two-time correlation function for the velocity on the other hand tends towards a stationary limit rapidly. This trend can also be seen for the corresponding memory kernels in figs. 26 and 27. Whereas the memory kernel for the displacement decreases in magnitude along the diagonal $t_1 = t_2$, which might be expected from the fact that the two-time correlation function for the displacement increases along this diagonal, the memory kernel for the velocity reaches a stationary limit rapidly again. However, the normalized memory kernel for the displacement
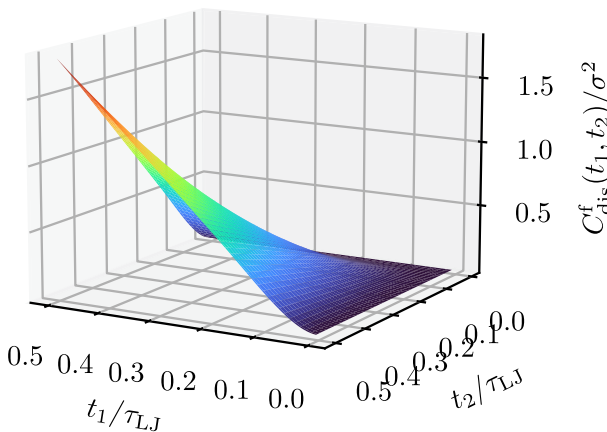
Fig. 24 Two-time correlation function for the displacement of the last particle in a polymer where an external force of strength $F = 50k_\mathrm{B}T/\sigma$ acts on the first particle of the same polymer. The polymer is in a three-dimensional polymer melt. (Coloured version available online)
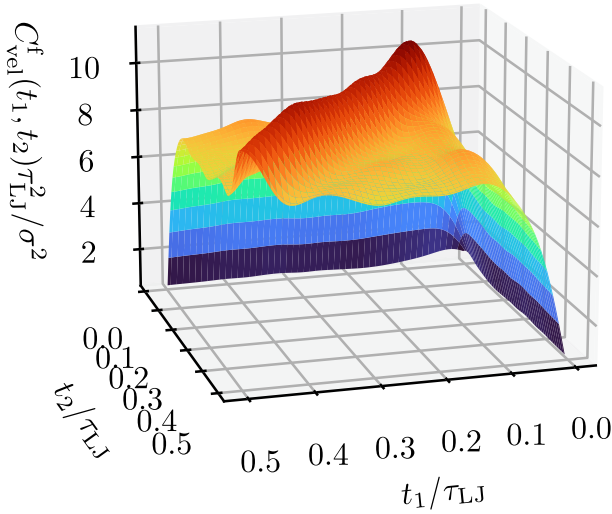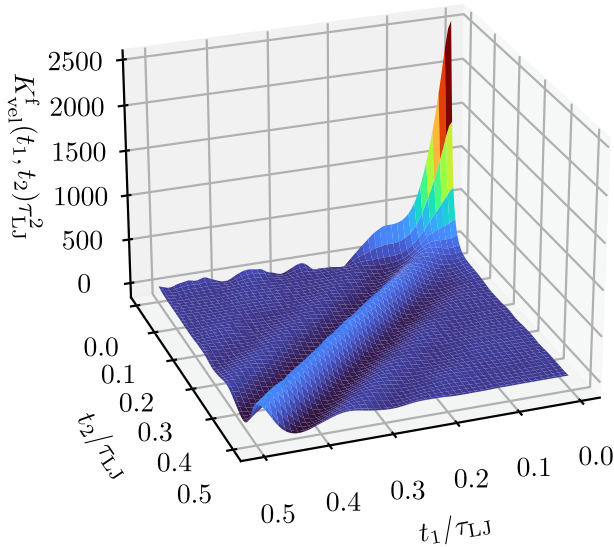
Fig. 25 Two-time correlation function for the velocity of the last particle in a polymer where an external force of strength $F = 50k_BT/\sigma$ acts on the first particle of the same polymer. The polymer is in a three-dimensional polymer melt. (Coloured version available online)
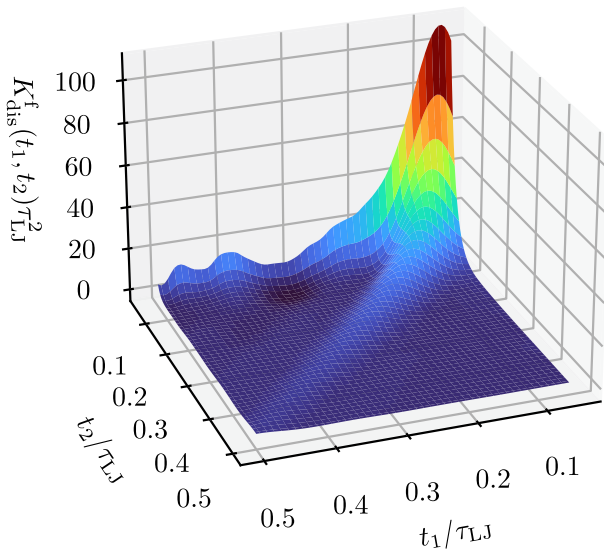
Fig. 26 Non-stationary memory kernel for the displacement of the last particle in a polymer where an external force of strength $F = 50k_BT/\sigma$ acts on the first particle of the same polymer. The polymer is in a three-dimensional polymer melt. Note that the memory kernel is not depicted for $t_1, t_2 < 0.05\tau_{LJ}$ because the memory kernel diverges for $t_1, t_2 \to 0$. (Coloured version available online)

Fig. 27 Non-stationary memory kernel for the velocity of the last particle in a polymer where an external force of strength $F = 50 k_\mathrm{B} T / \sigma$ acts on the first particle of the same polymer. The polymer is in a three-dimensional polymer melt. (Coloured version available online)

as shown in fig. 16 reaches a stationary limit. Thus, all slices of memory kernels shown in figs. 16 and 17 are representative for their shape at late times.

Data Availability The data that support the findings of this study are available from the corresponding author upon reasonable request.

Declarations

Conflict of interest The authors have no relevant financial or non-financial interests to disclose.

References

1. Mori, H.: Transport, collective motion, and Brownian motion. Prog. Theor. Phys. **33**, 423 (1965). https://doi.org/10.1143/PTP.33.423

2. Zwanzig, R.: Ensemble method in the theory of irreversibility. J. Chem. Phys. **33**, 1338 (1960). https://doi.org/10.1063/1.1731409

3. Zwanzig, R.: Memory effects in irreversible thermodynamics. Phys. Rev. **124**, 983 (1961). https://doi.org/10.1103/PhysRev.124.983

4. Rouse, P.E.: A theory of the linear viscoelastic properties of dilute solutions of coiling polymers. J. Chem. Phys. **21**, 1272 (1953). https://doi.org/10.1063/1.1699180

5. Kim, J., Sawada, I.: Dynamics of a harmonic oscillator on the Bethe lattice. Phys. Rev. E **61**, R2172 (2000). https://doi.org/10.1103/PhysRevE.61.R2172

6. Hajnal, D., Schilling, R.: Delocalization-localization transition due to anharmonicity. Phys. Rev. Lett. **101**, 124101 (2008). https://doi.org/10.1103/PhysRevLett.101.124101

7. Plyukhin, A.V.: Non-clausius heat transfer: the method of the nonstationary Langevin equation. Phys. Rev. E **102**, 052119 (2020). https://doi.org/10.1103/physreve.102.052119

8. Cubero, D., Yaliraki, S.N.: Inhomogeneous multiscale dynamics in harmonic lattices. J. Chem. Phys. **122**, 034108 (2005). https://doi.org/10.1063/1.1829253

9. Adelman, S.A., Doll, J.D.: Generalized langevin equation approach for atom/solid-surface scattering: collinear atom/harmonic chain model. J. Chem. Phys. **61**, 4242 (1974). https://doi.org/10.1063/1.1681723

10. Jung, B., Jung, G.: Dynamic coarse-graining of linear and non-linear systems: Mori-Zwanzig formalism and beyond. J. Chem. Phys. (2023). https://doi.org/10.1063/5.0165541

11. Wittmann, H.-P., Fredrickson, G.H.: Projection of the rouse model onto macroscopic equations of motion for polymers under shear. J. Phys. I France **4**, 1791 (1994). https://doi.org/10.1051/jp1:1994221

12. Maes, C., Thomas, S.R.: From langevin to generalized langevin equations for the nonequilibrium rouse model. Phys. Rev. E **87**, 022145 (2013). https://doi.org/10.1103/PhysRevE.87.022145

13. Potestio, R., Peter, C., Kremer, K.: Computer simulations of soft matter: linking the scales. Entropy **16**, 4199 (2014). https://doi.org/10.3390/e16084199

14. Li, Z., Lee, H.S., Darve, E., Karniadakis, G.E.: Computing the non-Markovian coarse-grained interactions derived from the Mori-Zwanzig formalism in molecular systems: Application to polymer melts. J. Chem. Phys. **146**, 014104 (2017). https://doi.org/10.1063/1.4973347

15. Deichmann, G., van der Vegt, N.F.A.: Bottom-up approach to represent dynamic properties in coarse-grained molecular simulations. J. Chem. Phys. (2018). https://doi.org/10.1063/1.5064369

16. Kempfer, K., Devémy, J., Dequidt, A., Couty, M., Malfreyt, P.: Development of coarse-grained models for polymers by trajectory matching. ACS Omega **4**, 5955 (2019). https://doi.org/10.1021/acsomega.9b00144

17. Jin, J., Pak, A.J., Durumeric, A.E.P., Loose, T.D., Voth, G.A.: Bottom-up coarse-graining: principles and perspectives. J. Chem. Theory Comput. **18**, 5759 (2022). https://doi.org/10.1021/acs.jctc.2c00643

18. Jin, J., Voth, G.A.: Statistical mechanical design principles for coarse-grained interactions across different conformational free energy surfaces. J. Phys. Chem. Lett. **14**, 1354 (2023). https://doi.org/10.1021/acs.jpclett.2c03844

19. Grabert, H.: Projection Operator Techniques in Nonequilibrium Statistical Mechanics, Springer Tracts in Modern Physics (Springer, Berlin, 2006) https://books.google.de/books?id=z5t0DgAAQBAJ

20. Klippenstein, V., Tripathy, M., Jung, G., Schmid, F., van der Vegt, N.F.A.: Introducing memory in coarse-grained molecular simulations. J. Phys. Chem. B **125**, 4931 (2021). https://doi.org/10.1021/acs.jpcb.1c01120

21. Meyer, H., Voigtmann, T., Schilling, T.: On the non-stationary generalized langevin equation. J. Chem. Phys. **147**, 214110 (2017). https://doi.org/10.1063/1.5006980

22. Meyer, H., Voigtmann, T., Schilling, T.: On the dynamics of reaction coordinates in classical, time-dependent, many-body processes. J. Chem. Phys. **150**, 174118 (2019). https://doi.org/10.1063/1.5090450

23. Meyer, H., Wolf, S., Stock, G., Schilling, T.: A numerical procedure to evaluate memory effects in non-equilibrium coarse-grained models. Adv. Theor. Simul. **4**, 2000197 (2020). https://doi.org/10.1002/adts.202000197

24. Widder, C., Koch, F., Schilling, T.: Generalized langevin dynamics simulation with non-stationary memory kernels: how to make noise. J. Chem. Phys. **157**, 194107 (2022). https://doi.org/10.1063/5.0127557

25. Forster, D.: Hydrodynamic Fluctuations, Broken Symmetry, and Correlation Functions. The Benjamin/Cummings Publishing Company, San Francisco (1975)

26. Snook, I.: Langevin and Generalised Langevin Approach to the Dynamics of Atomic, Polymeric and Colloidal Systems. Elsevier, Amsterdam (2006)

27. Shin, H.K., Kim, C., Talkner, P., Lee, E.K.: Brownian motion from molecular dynamics. Chem. Phys. **375**, 316 (2010). https://doi.org/10.1016/j.chemphys.2010.05.019

28. te Vrugt, M., Wittkowski, R.: Projection operators in statistical mechanics: a pedagogical approach. Eur. J. Phys. (2020). https://doi.org/10.1088/1361-6404/ab8e28

29. Florencio, J., Lee, M.H.: Exact time evolution of a classical harmonic-oscillator chain. Phys. Rev. A **31**, 3231 (1985). https://doi.org/10.1103/PhysRevA.31.3231
30. Kupferman, R., Stuart, A.: Fitting sde models to nonlinear kac-zwanzig heat bath models. Physica D **199**, 279 (2004)
31. Wang, Z.: Fast algorithms for the discrete w transform and for the discrete Fourier transform. IEEE Trans. Acoust. Speech Signal Process. **32**, 803 (1984). https://doi.org/10.1109/TASSP.1984.1164399
32. Britanak, V., Yip, P., Rao, K.: Discrete Cosine and Sine Transforms: General Properties, Fast Algorithms and Integer Approximations (Elsevier Science, Amsterdam, 2010) https://books.google.de/books?id=iRlQHcK-r_kC
33. Rouse, P.E.: A theory of the linear viscoelastic properties of dilute solutions of coiling polymers. J. Chem. Phys. **21**, 1272 (1953). https://doi.org/10.1063/1.1699180
34. Tian, X., Xu, X., Chen, Y., Chen, J., Xu, W.-S.: Explicit analytical form for memory kernel in the generalized Langevin equation for end-to-end vector of Rouse chains. J. Chem. Phys. (2022). https://doi.org/10.1063/5.0124925
35. Vandebroek, H., Vanderzande, C.: On the generalized Langevin equation for a Rouse bead in a nonequilibrium bath. J. Stat. Phys. **167**, 14 (2017). https://doi.org/10.1007/s10955-017-1734-x
36. Maes, C., Thomas, S.R.: From Langevin to generalized Langevin equations for the nonequilibrium Rouse model. Phys. Rev. E **87**, 022145 (2013). https://doi.org/10.1103/physreve.87.022145
37. Wong, C.P.J., Choi, P.: Velocity time correlation function of a Rouse chain. Comput. Mater. Sci. **155**, 320 (2018). https://doi.org/10.1016/j.commatsci.2018.08.042
38. Doi, M., Edwards, S.F.: The Theory of Polymer Dynamics, p. 406. Oxford University Press, Oxford (1988)
39. Keesman, R., Barkema, G.T., Panja, D.: Dynamical eigenmodes of a polymerized membrane. J. Stat. Mech: Theory Exp. **2013**, P04009 (2013). https://doi.org/10.1088/1742-5468/2013/04/p04009
40. Kalathi, J.T., Kumar, S.K., Rubinstein, M., Grest, G.S.: Rouse mode analysis of chain relaxation in homopolymer melts. Macromolecules **47**, 6925 (2014). https://doi.org/10.1021/ma500900b
41. W. R. Inc., Mathematica, Version 13.0, Champaign (2021)
42. Amati, G., Meyer, H., Schilling, T.: Memory effects in the fermi-pasta-ulam model. J. Stat. Phys. **174**, 219 (2019). https://doi.org/10.1007/s10955-018-2207-6
43. Weeks, J.D., Chandler, D., Andersen, H.C.: Role of repulsive forces in determining the equilibrium structure of simple liquids. J. Chem. Phys. **54**, 5237 (1971). https://doi.org/10.1063/1.1674820
44. Berkowitz, M., Morgan, J.D., McCammon, J.A.: Generalized Langevin dynamics simulations with arbitrary time-dependent memory kernels. J. Chem. Phys. **78**, 3256 (1983). https://doi.org/10.1063/1.445244
45. Español, P., Zúñiga, I.: Force autocorrelation function in Brownian motion theory. J. Chem. Phys. **98**, 574 (1993). https://doi.org/10.1063/1.464599
46. Español, P., de la Torre, J.A., Duque-Zumajo, D.: Solution to the plateau problem in the Green–Kubo formula. Phys. Rev. E **99**, 022126 (2019). https://doi.org/10.1103/physreve.99.022126
47. Louis, A.A., Bolhuis, P.G., Hansen, J.P., Meijer, E.J.: Can polymer coils be modeled as "soft colloids"? Phys. Rev. Lett. **85**, 2522 (2000). https://doi.org/10.1103/PhysRevLett.85.2522
48. Kremer, K., Grest, G.S.: Dynamics of entangled linear polymer melts: a molecular-dynamics simulation. J. Chem. Phys. **92**, 5057 (1990)
49. Panja, D.: Anomalous polymer dynamics is non-Markovian: memory effects and the generalized Langevin equation formulation. J. Stat. Mech: Theory Exp. **2010**, P06011 (2010). https://doi.org/10.1088/1742-5468/2010/06/p06011

Publisher's Note Springer Nature remains neutral with regard to jurisdictional claims in published maps and institutional affiliations.